Efficient implementation of the *GW* approximation within the all-electron FLAPW method

Christoph Friedrich[*] and Stefan Blügel

Institut für Festkörperforschung and Institute for Advanced Simulation, Forschungszentrum Jülich, 52425 Jülich, Germany

Arno Schindlmayr

Department Physik, Universität Paderborn, 33095 Paderborn, Germany

We present an implementation of the *GW* approximation for the electronic self-energy within the full-potential linearized augmented-plane-wave (FLAPW) method. The algorithm uses an all-electron mixed product basis for the representation of response matrices and related quantities. This basis is derived from the FLAPW basis and is exact for wave-function products. The correlation part of the self-energy is calculated on the imaginary-frequency axis with a subsequent analytic continuation to the real axis. As an alternative we can perform the frequency convolution of the Green function *G* and the dynamically screened Coulomb interaction *W* explicitly by a contour integration. The singularity of the bare and screened interaction potentials gives rise to a numerically important self-energy contribution, which we treat analytically to achieve good convergence with respect to the **k**-point sampling. As numerical realizations of the *GW* approximation typically suffer from the high computational expense required for the evaluation of the nonlocal and frequency-dependent self-energy, we demonstrate how the algorithm can be made very efficient by exploiting spatial and time-reversal symmetry as well as by applying an optimization of the mixed product basis that retains only the numerically important contributions of the electron-electron interaction. This optimization step reduces the basis size without compromising the accuracy and accelerates the code considerably. Furthermore, we demonstrate that one can employ an extrapolar approximation for high-lying states to reduce the number of empty states that must be taken into account explicitly in the construction of the polarization function and the self-energy. We show convergence tests, CPU timings, and results for prototype semiconductors and insulators as well as ferromagnetic nickel.

I. INTRODUCTION

Many-body perturbation theory with the *GW* approximation for the electronic self-energy offers a well-established approach for the computation of excited electronic states from first principles.[1] In principle, the electronic self-energy incorporates all many-body exchange and correlation effects beyond the Hartree theory. The *GW* approximation contains the electronic exchange exactly while the screening is treated at the level of the random-phase approximation,[2] where non-interacting electron-hole ring diagrams are summed to all orders. This makes the *GW* approximation particularly suited for weakly to moderately correlated systems.

After its theoretical foundation by Hedin[3] in 1965 it was not before the middle of the 1980s that the computational treatment of real materials became feasible. In spite of approximations in the numerical treatment that were necessary due to the lack of computer power, the first results were very promising. In these works,[4–7] it could be shown that the theoretical band gap fell within a margin of 0.1 eV from the experimental value for covalently bonded semiconductors. After these pioneering studies, the *GW* approximation has evolved into the method of choice for calculating electronic excitations in solid-state systems.

So far, most codes still rely on the pseudopotential approximation, which restricts the range of materials that can be examined. Transition-metal compounds and oxides, in particular, cannot be treated efficiently in this approach. Two early all-electron calculations using the *GW* approximation

were carried out by Hamada *et al.*[8] for Si and by Aryasetiawan[9] for Ni, both within the linearized augmented-plane-wave (LAPW) method. However, only very recently were further all-electron implementations reported, based on the full-potential LAPW (FLAPW) (Refs. 10 and 11), the linearized muffin-tin orbital (LMTO) (Refs. 12–14), the projector-augmented-wave (PAW) (Refs. 15–17), and the Korringa-Kohn-Rostoker method (Ref. 18) together with applications to a larger variety of systems.

While the calculation of *GW* band structures for small systems has become routine, the scientific community is increasingly interested in larger and more complex systems, such as multicomponent materials, artificial heterostructures, defects, interfaces, surfaces, clusters, and nanowires. In codes using periodic boundary conditions, such systems must be treated in supercell geometries often exceeding 100 atoms. The main obstacle in applying the *GW* approximation in supercell calculations is the considerable demand of computation time and memory. This is especially true for all-electron methods, where the rapid oscillations close to the atomic nuclei make the usage of the fast Fourier transformation impossible. Therefore, all-electron *GW* calculations for large systems have so far been prohibitive. In this paper, we describe numerical algorithms and approximations that make all-electron *GW* implementations efficient and bring large supercell calculations into reach.

The nonlocality of the self-energy operator is the main reason for the large computational effort needed in *GW* calculations. It leads to convolutions in reciprocal space, i.e.,

summations over the Brillouin zone (BZ), which is sampled by a finite set of **k** points. Furthermore, the bare electron-electron interaction diverges at the center of the BZ, giving rise to a corresponding divergence and an anisotropy in the dynamically screened interaction at **k** = **0**. A thorough treatment of the Γ point is hence crucial for an accurate and efficient BZ summation. Previous all-electron implementations[10,19] of many-body perturbation theory have often bypassed this problem by reverting to a plane-wave basis for the Coulomb potential and related propagators such as the dielectric function but such a projection leads to a loss of accuracy because it cannot resolve the rapid oscillations of the orbitals close to the atomic nuclei without a prohibitively large basis set. As a consequence, physical effects such as core polarization are inadequately described. In an alternative approach, the so-called offset-Γ method, an auxiliary **k**-point mesh that is shifted from the origin by a small but finite amount is employed.[12,16] In this way, the singularity is avoided but the use of additional meshes increases the numerical cost; even in the most favorable case, for cubic symmetry, the number of **k** points must at least be doubled. Furthermore, the convergence of BZ integrals involving the Coulomb matrix, for example, for the *GW* self-energy, may be slow with respect to the **k**-point sampling due to the approximate treatment of the quantitatively important region near the zone center. In this work, we take the Γ point explicitly into account and employ an analytical treatment of the Coulomb singularity. We use a recently developed procedure[20] to transform the all-electron basis for the interaction potentials, the so-called mixed product basis,[12] in such a way that the divergence is restricted to a single matrix element, which allows a treatment similar to a pure plane-wave basis set.

The numerical cost of the BZ convolutions can be reduced considerably by employing spatial and time-reversal symmetries. Not only can the **k** dependence of response quantities be confined to the irreducible wedge of the BZ but also the convolutions over the reciprocal space can be restricted to an extended irreducible zone without loss of accuracy. Furthermore, in the presence of inversion symmetry, the all-electron mixed product basis can be transformed in such a way that response matrices become real instead of complex, which again reduces the numerical cost in terms of computation time and memory demand.

We further demonstrate that we can afford to truncate the number of basis functions considerably in the calculation of the correlation part of the self-energy. This is achieved by a basis transformation that diagonalizes the Coulomb matrix. Eigenvectors with small eigenvalues then correspond to unimportant scattering contributions, which can be neglected in a systematic way. This leads to an optimization of the basis set and thus to a speed up of the computation.

The paper is organized as follows. In Sec. II, we give a brief introduction to the *GW* approximation. In Sec. III, we describe our all-electron implementation in detail: the mixed product basis and its optimization, the **k**-point set, the treatment of the Γ-point divergence, and the usage of spatial and time-reversal symmetry. Section IV reports convergence tests for Si and SrTiO$_3$ as well as fundamental *GW* band gaps for a variety of semiconductors and insulators. In addition, re-

sults for the localized 3*d* states of GaAs and ferromagnetic Ni as an example of a 3*d* transition metal are discussed. In order to illustrate the efficiency of the code, we also show CPU timings for diamond in supercell geometries containing up to 128 atoms. Finally we summarize our conclusions in Sec. V.

II. *GW* APPROXIMATION

Angle-resolved photoelectron spectroscopy is the prime experimental technique for the measurement of the electronic band structure of crystalline materials. The excitations measured in photoelectron spectroscopy involve electron ejection or injection and thus imply a change in the particle number by one. The corresponding many-body excitation energies $E_{n\mathbf{q}}^{\sigma}$, where **q** is the wave vector, *n* the band index, and σ the electron spin, define the pole structure of the one-particle Green function,

$$G^{\sigma}(\mathbf{r},\mathbf{r}';\omega) = \sum_{\mathbf{q}}^{\mathrm{BZ}} \sum_{n}^{\mathrm{all}} \frac{\psi_{n\mathbf{q}}^{\sigma}(\mathbf{r})\psi_{n\mathbf{q}}^{\sigma*}(\mathbf{r}')}{\omega - E_{n\mathbf{q}}^{\sigma} + E_0 + i\eta \, \mathrm{sgn}(E_{n\mathbf{q}}^{\sigma} - E_0)}$$

(1)

with the quasiparticle wave functions $\psi_{n\mathbf{q}}^{\sigma}(\mathbf{r})$ and the many-body ground-state energy E_0. Here and in the following the number η is infinitesimal, real, and positive, and by a sum over Bloch vectors **q**, we always mean an integration over the BZ multiplied by the density of **q** points $V/(8\pi^3)$ with the crystal volume *V*. Hartree atomic units are used throughout except where noted otherwise.

The quasiparticle wave functions $\psi_{n\mathbf{q}}^{\sigma}(\mathbf{r})$ and energies $E_{n\mathbf{q}}^{\sigma}$ obey a set of one-particle differential equations,

$$\hat{h}_0 \psi_{n\mathbf{q}}^{\sigma}(\mathbf{r}) + \int \left[\Sigma_{\mathrm{xc}}^{\sigma}(\mathbf{r},\mathbf{r}';E_{n\mathbf{q}}) - v_{\mathrm{xc}}^{\sigma}(\mathbf{r}')\delta(\mathbf{r}-\mathbf{r}') \right] \psi_{n\mathbf{q}}^{\sigma}(\mathbf{r}')d^3r'$$

$$= E_{n\mathbf{q}}^{\sigma} \psi_{n\mathbf{q}}^{\sigma}(\mathbf{r}),$$

(2)

the so-called quasiparticle equations, where $\hat{h}_0$ is the Kohn-Sham (KS) Hamiltonian,

$$\hat{h}_0 = -\frac{1}{2}\nabla^2 + v_{\mathrm{ext}}(\mathbf{r}) + v_{\mathrm{H}}(\mathbf{r}) + v_{\mathrm{xc}}^{\sigma}(\mathbf{r})$$

(3)

with the external, Hartree, and exchange-correlation potentials, respectively,[21] and $\Sigma_{\mathrm{xc}}^{\sigma}(\mathbf{r},\mathbf{r}';\omega)$ is the nonlocal, non-Hermitian, and energy-dependent exchange-correlation self-energy.

In practical implementations one usually treats the integral operator on the left-hand side of Eq. (2) as a small perturbation. In first order, the quasiparticle energies are then given by the nonlinear equation,

$$E_{n\mathbf{q}}^{\sigma} = \epsilon_{n\mathbf{q}}^{\sigma} + \langle \varphi_{n\mathbf{q}}^{\sigma} | \Sigma_{\mathrm{xc}}^{\sigma}(E_{n\mathbf{q}}^{\sigma}) - v_{\mathrm{xc}}^{\sigma} | \varphi_{n\mathbf{q}}^{\sigma} \rangle$$

(4)

with the KS wave functions $\varphi_{n\mathbf{q}}^{\sigma}$ and energies $\epsilon_{n\mathbf{q}}^{\sigma}$. This is equivalent to neglecting off-diagonal elements of $\Sigma_{\mathrm{xc}}^{\sigma}(E_{n\mathbf{q}}^{\sigma}) - v_{\mathrm{xc}}^{\sigma}$ in the basis of the KS wave functions. For the self-energy, we use the *GW* approximation,

$$\Sigma_{\mathrm{xc}}^\sigma(\mathbf{r},\mathbf{r}';\omega) = \frac{i}{2\pi}\int G_0^\sigma(\mathbf{r},\mathbf{r}';\omega+\omega')W(\mathbf{r},\mathbf{r}';\omega')e^{i\eta\omega'}d\omega',$$

$$(5)$$

which constitutes the first-order term of the self-energy expansion in powers of the dynamically screened Coulomb interaction W. Here

$$G_0^\sigma(\mathbf{r},\mathbf{r}';\omega) = \sum_{\mathbf{q}}^{\mathrm{BZ}}\sum_n^{\mathrm{all}} \frac{\varphi_{n\mathbf{q}}^\sigma(\mathbf{r})\varphi_{n\mathbf{q}}^{\sigma*}(\mathbf{r}')}{\omega - \epsilon_{n\mathbf{q}}^\sigma + i\eta\,\mathrm{sgn}(\epsilon_{n\mathbf{q}}^\sigma)} \qquad (6)$$

is the time-ordered KS Green function, which is obtained from Eq. (1) by replacing $\psi_{n\mathbf{q}}^\sigma(\mathbf{r})$ with the KS wave functions $\varphi_{n\mathbf{q}}^\sigma(\mathbf{r})$ and $E_{n\mathbf{q}}^\sigma - E_0$ with the KS energies $\epsilon_{n\mathbf{q}}^\sigma$ measured from the Fermi energy.

The dynamically screened interaction obeys a Dyson-type integral equation,

$$W(\mathbf{r},\mathbf{r}';\omega) = v(\mathbf{r},\mathbf{r}') + \int v(\mathbf{r},\mathbf{r}'')P(\mathbf{r}'',\mathbf{r}''';\omega)$$
$$\times W(\mathbf{r}''',\mathbf{r}';\omega)d^3r''d^3r''' \qquad (7)$$

with the bare Coulomb interaction $v(\mathbf{r},\mathbf{r}')=1/|\mathbf{r}-\mathbf{r}'|$ and the polarization function $P(\mathbf{r},\mathbf{r}';\omega)$, for which we employ the random-phase approximation,[2]

$$P(\mathbf{r},\mathbf{r}';\omega) = -\frac{i}{2\pi}\sum_\sigma \int_{-\infty}^\infty G_0^\sigma(\mathbf{r},\mathbf{r}';\omega')$$
$$\times G_0^\sigma(\mathbf{r}',\mathbf{r};\omega'-\omega)e^{i\eta\omega'}d\omega'$$
$$= \sum_\sigma \sum_{\mathbf{q},\mathbf{k}}^{\mathrm{BZ}} \sum_n^{\mathrm{occ}} \sum_{n'}^{\mathrm{unocc}} \varphi_{n\mathbf{q}}^{\sigma*}(\mathbf{r})\varphi_{n'\mathbf{k}}^\sigma(\mathbf{r})\varphi_{n\mathbf{q}}^\sigma(\mathbf{r}')\varphi_{n'\mathbf{k}}^{\sigma*}(\mathbf{r}')$$
$$\times \left(\frac{1}{\omega + \epsilon_{n\mathbf{q}}^\sigma - \epsilon_{n'\mathbf{k}}^\sigma + i\eta} - \frac{1}{\omega - \epsilon_{n\mathbf{q}}^\sigma + \epsilon_{n'\mathbf{k}}^\sigma - i\eta} \right).$$

$$(8)$$

This approximation corresponds to time-dependent Hartree theory and thus neglects exchange-correlation (e.g., excitonic) effects in the dynamical screening. With the dielectric function,

$$\varepsilon(\mathbf{r},\mathbf{r}';\omega) = \delta(\mathbf{r}-\mathbf{r}') - \int v(\mathbf{r},\mathbf{r}'')P(\mathbf{r}'',\mathbf{r}';\omega)d^3r'', \quad (9)$$

we can write the screened interaction in the closed form,

$$W(\mathbf{r},\mathbf{r}';\omega) = \int \varepsilon^{-1}(\mathbf{r},\mathbf{r}'';\omega)v(\mathbf{r}'',\mathbf{r}')d^3r''. \qquad (10)$$

Many-body screening effects obviously enter with the second term of Eq. (9) into the formalism. In fact, if we write the screened interaction as a sum of the bare interaction and a remainder,

$$W(\mathbf{r},\mathbf{r}';\omega) = v(\mathbf{r},\mathbf{r}') + W^{\mathrm{c}}(\mathbf{r},\mathbf{r}';\omega), \qquad (11)$$

then the self-energy [Eq. (5)] decomposes into the terms

$$\Sigma_{\mathrm{x}}^\sigma(\mathbf{r},\mathbf{r}') = \frac{i}{2\pi}\int G_0^\sigma(\mathbf{r},\mathbf{r}';\omega+\omega')v(\mathbf{r},\mathbf{r}')e^{i\eta\omega'}d\omega' \quad (12)$$

and

$$\Sigma_{\mathrm{c}}^\sigma(\mathbf{r},\mathbf{r}';\omega) = \frac{i}{2\pi}\int G_0^\sigma(\mathbf{r},\mathbf{r}';\omega+\omega')W^{\mathrm{c}}(\mathbf{r},\mathbf{r}';\omega')d\omega',$$

$$(13)$$

which are identified as the exchange and the correlation contributions to the electronic self-energy, respectively. We note that the exponential factor allows to close the integration path over the upper complex half plane in Eq. (12). As $W^{\mathrm{c}}(\mathbf{r},\mathbf{r}';\omega)$ falls off quickly enough with increasing frequencies, we may take the limit $\eta\to 0$ before integrating in Eq. (13).

In the next section, we discuss several aspects of the implementation that are important for the computational efficiency. The numerical procedure is based on an auxiliary all-electron basis set, the mixed product basis, in which the previous integral equations become matrix equations that can be implemented easily. We have already explained this basis set in detail in a previous publication[20] and only sketch the basic ideas here.

III. IMPLEMENTATION

A. FLAPW method

In the FLAPW method,[22] space is partitioned into non-overlapping atom-centered muffin tin (MT) spheres and the interstitial region (IR). The core-electron wave functions, which are (predominantly) confined to the MT spheres, are directly obtained from a solution of the fully relativistic Dirac equation. The valence-electron wave functions with spin σ are expanded in interstitial plane waves (IPWs) in the IR and numerical functions $u_{almp}^\sigma(\mathbf{r})=u_{alp}^\sigma(r)Y_{lm}(\mathbf{e_r})$ inside the MT sphere of atom a, where $\mathbf{r}$ is measured from the MT center located at $\mathbf{R}_a$. These numerical functions comprise solutions of the KS equation for the spherically averaged effective potential for $p=0$ and their first energy derivatives $u_{alm1}^\sigma(\mathbf{r})=\partial u_{alm0}^\sigma(\mathbf{r})/\partial\epsilon_{al}^\sigma$ for $p=1$ evaluated at suitably chosen energy parameters ϵ_{al}^σ, and $Y_{lm}(\mathbf{e_r})$ denote the spherical harmonics. The notation $\mathbf{e_r}=\mathbf{r}/r$ with $r=|\mathbf{r}|$ indicates the unit vector in the direction of $\mathbf{r}$. In a given unit cell, the KS wave function at a wave vector $\mathbf{k}$ with band index n and spin σ is then given by

$$\varphi_{n\mathbf{k}}^\sigma(\mathbf{r})$$
$$= \begin{cases} \dfrac{1}{\sqrt{N}}\displaystyle\sum_{l=0}^{l_{\max}}\sum_{m=-l}^{l}\sum_{p=0}^{1} A_{almp}^{n\mathbf{k}\sigma}u_{almp}^\sigma(\mathbf{r}-\mathbf{R}_a) & \text{if } \mathbf{r}\in\mathrm{MT}(a) \\[2ex] \dfrac{1}{\sqrt{V}}\displaystyle\sum_{|\mathbf{k}+\mathbf{G}|\leq G_{\max}} c_{\mathbf{G}}^{n\mathbf{k}\sigma}e^{i(\mathbf{k}+\mathbf{G})\cdot\mathbf{r}} & \text{if } \mathbf{r}\in\mathrm{IR} \end{cases}$$

$$(14)$$

with the crystal volume V, the number of unit cells N, and cutoff values $l_{\max}$ and $G_{\max}$. The coefficients $A_{almp}^{n\mathbf{k}\sigma}$ are determined by the requirement that the wave function is continu-

ous in value and first radial derivative at the MT sphere boundaries. If desired, additional local orbitals for semicore states[23] or higher energy derivatives[24] can be incorporated by allowing $p \geq 2$. We use the FLEUR code[25] for the density-functional theory (DFT) calculations.

B. Mixed product basis (MPB)

If the integral equations of Sec. II are rewritten in an auxiliary basis set, they become matrix equations, which can easily be treated in a computer code using standard linear-algebra libraries. Equation (8) already indicates that this auxiliary basis set should accurately represent wave-function products. This is generally true for all quantities that involve two spatial coordinates and thus couple two incoming and outgoing electrons with each other.

The FLAPW method uses continuous basis functions that are defined everywhere in space but have a different mathematical representation in the MT spheres and the IR. For the expansion of wave-function products, however, it is better to employ two separate sets of functions that are defined only in one of the spatial regions and zero in the other. In this way, linear dependences that occur only in one region can easily be eliminated, which overall leads to a smaller and more efficient basis. The resulting combined set of functions is called the MPB.[12]

Inside the MT spheres, the MPB must accurately describe the products $u^{\sigma*}_{almp}(\mathbf{r})u^{\sigma}_{al'm'p'}(\mathbf{r})$. The angular parts $Y^*_{lm}(\mathbf{e_r})Y_{l'm'}(\mathbf{e_r})$ can be represented by linear combinations of spherical harmonics $Y_{LM}(\mathbf{e_r})$ with $|l-l'| \leq L \leq l+l'$ and $-L \leq M \leq L$ while the radial parts define a set of product functions $U^{\sigma}_{aLP}(r) = u^{\sigma}_{alp}(r)u^{\sigma}_{al'p'}(r)$, where the index P counts all possible combinations of l, l', p, and p'. We emphasize that, in general, the latter lie outside the vector space spanned by the original numerical basis functions $u^{\sigma}_{alp}(r)$. Initially, the set $\{U^{\sigma}_{aLP}(r)\}$ is neither normalized nor orthogonal and usually has a high degree of (near) linear dependence. An effective procedure to remove these (near) linear dependences is to diagonalize the overlap matrix and to retain only those eigenvectors whose eigenvalues exceed a specified threshold value.[26] In this way, the MT functions become orthonormalized. By using both spin-up and spin-down products in the construction of the overlap matrix, we make the resulting basis spin independent. In practice, the basis set is reduced further by introducing a cutoff value $L_{\max}$ for the angular quantum number. On the other hand, it must be supplemented with a constant MT function for each atom in the unit cell, which is later needed to represent the eigenfunction that corresponds to the divergent eigenvalue of the Coulomb matrix in the limit $\mathbf{k} \to \mathbf{0}$. From the resulting MT functions $M_{aLMP}(\mathbf{r}) = M_{aLP}(r)Y_{LM}(\mathbf{e_r})$, we formally construct Bloch functions.

In the IR, we use a set of IPWs with a cutoff $G'_{\max} \leq 2G_{\max}$ in reciprocal space since the product of two IPWs yields another IPW. Together with the MT functions, we thus obtain the MPB $\{M^{\mathbf{k}}_I(\mathbf{r})\} = \{M_{aLMP}(\mathbf{r}), M^{\mathbf{k}}_{\mathbf{G}}(\mathbf{r})\}$ for the representation of wave-function products. Unlike the MT functions, which have been explicitly orthonormalized, the IPWs are not orthogonal to each other; the elements of their overlap matrix can be calculated analytically and are given by

$$\langle M^{\mathbf{k}}_{\mathbf{G}}|M^{\mathbf{k}'}_{\mathbf{G}'}\rangle = \delta_{\mathbf{k}\mathbf{k}'}O_{\mathbf{G}\mathbf{G}'}(\mathbf{k}) = \delta_{\mathbf{k}\mathbf{k}'}\Theta_{\mathbf{G}-\mathbf{G}'}, \quad (15)$$

where $\Theta_{\mathbf{G}}$ are the Fourier coefficients of the step function, which equals 1 in the IR and 0 in the MT spheres. We also define a second set, the biorthogonal set,

$$\widetilde{M}^{\mathbf{k}}_{\mathbf{G}}(\mathbf{r}) = \sum_{\mathbf{G}'} M^{\mathbf{k}}_{\mathbf{G}'}(\mathbf{r})O^{-1}_{\mathbf{G}'\mathbf{G}}(\mathbf{k}). \quad (16)$$

It fulfills the identities

$$\langle \widetilde{M}^{\mathbf{k}}_I|M^{\mathbf{k}}_J\rangle = \langle M^{\mathbf{k}}_I|\widetilde{M}^{\mathbf{k}}_J\rangle = \delta_{IJ}, \quad (17a)$$

$$\sum_I |M^{\mathbf{k}}_I\rangle\langle \widetilde{M}^{\mathbf{k}}_I| = \sum_I |\widetilde{M}^{\mathbf{k}}_I\rangle\langle M^{\mathbf{k}}_I| = 1, \quad (17b)$$

where the completeness relation is only valid in the subspace spanned by the MPB, though. As the MT functions and the IPWs are defined in different regions of space and the MT functions are orthonormal, only the IPWs overlap in a nontrivial way. It should be noted that the overlap matrix is $\mathbf{k}$ dependent because the size of the MPB varies for different $\mathbf{k}$ vectors.

In general, the matrix representation of real operators in an arbitrary complex basis $\{f_\mu(\mathbf{r})\}$ is Hermitian. If the system has inversion symmetry and the basis functions fulfill

$$f_\mu(-\mathbf{r}) = f^*_\mu(\mathbf{r}), \quad (18)$$

it is easy to show that the matrices become real symmetric. Of course, this reduces the computational cost considerably, in terms of both memory consumption and computation time. However, according to the current definition only the IPWs fulfill Eq. (18) while the MT functions do not. For a system with inversion symmetry, we hence apply a unitary transformation of the MT functions such that Eq. (18) is satisfied.[27] In the following, it is understood that all quantities are represented in this symmetrized basis if inversion symmetry is present.

C. Formulation in the MPB

In this section, we reformulate the equations of Sec. II by projecting onto the MPB and exploiting the identities in Eq. (16). Because of the exponential factor in Eq. (12), we can formally close the frequency integration contour with an infinite half circle over the positive imaginary plane without changing the value of the integral. This contour integral then equals the sum over the residues of the poles of the Green function. The expectation value of the exchange term with respect to a wave function $\varphi^{\sigma}_{n\mathbf{q}}(\mathbf{r})$ yields the well-known Hartree-Fock expression

$$\langle \varphi^{\sigma}_{n\mathbf{q}}|\Sigma^{\sigma}_x|\varphi^{\sigma}_{n\mathbf{q}}\rangle = -\sum_{\mathbf{k}}^{\text{BZ}}\sum_{n'}^{\text{occ}}\sum_{I,J} v_{IJ}(\mathbf{k})$$
$$\times \langle \varphi^{\sigma}_{n'\mathbf{q}+\mathbf{k}}|\varphi^{\sigma}_{n\mathbf{q}}\widetilde{M}^{\mathbf{k}}_I\rangle\langle \widetilde{M}^{\mathbf{k}}_J\varphi^{\sigma}_{n\mathbf{q}}|\varphi^{\sigma}_{n'\mathbf{q}+\mathbf{k}}\rangle \quad (19)$$

with the projections

$$\langle \widetilde{M}_I^{\mathbf{k}} \varphi_{n\mathbf{q}}^{\sigma} | \varphi_{n'\mathbf{q+k}}^{\sigma} \rangle = \int \widetilde{M}_I^{\mathbf{k}^*}(\mathbf{r}) \varphi_{n\mathbf{q}}^{\sigma^*}(\mathbf{r}) \varphi_{n'\mathbf{q+k}}^{\sigma}(\mathbf{r}) d^3r \quad (20)$$

and the Coulomb matrix[20]

$$v_{IJ}(\mathbf{k}) = \langle M_I^{\mathbf{k}} | v | M_J^{\mathbf{k}} \rangle = \int \int \frac{M_I^{\mathbf{k}^*}(\mathbf{r}) M_J^{\mathbf{k}}(\mathbf{r}')}{|\mathbf{r} - \mathbf{r}'|} d^3r \, d^3r'. \quad (21)$$

The sum over the occupied states also comprises the core states, which give an important contribution to the exchange self-energy. Its evaluation is simplified considerably by the fact that the core states can be treated as dispersionless bands. We use a formalism derived by Dagens and Perrot.[28] An efficient scheme for the calculation of the full nonlocal Fock exchange potential including off-diagonal elements will be presented elsewhere.[27]

With the projections [Eq. (20)], we readily obtain the representation of the polarization function,

$$P_{IJ}(\mathbf{k}, \omega)$$
$$= \sum_{\sigma}^{} \sum_{\mathbf{q}}^{\mathrm{BZ}} \sum_{n}^{\mathrm{occ}} \sum_{n'}^{\mathrm{unocc}} \langle \widetilde{M}_I^{\mathbf{k}} \varphi_{n\mathbf{q}}^{\sigma} | \varphi_{n'\mathbf{q+k}}^{\sigma} \rangle \langle \varphi_{n'\mathbf{q+k}}^{\sigma} | \varphi_{n\mathbf{q}}^{\sigma} \widetilde{M}_J^{\mathbf{k}} \rangle$$
$$\times \left(\frac{1}{\omega + \epsilon_{n\mathbf{q}}^{\sigma} - \epsilon_{n'\mathbf{q+k}}^{\sigma} + i\eta} - \frac{1}{\omega - \epsilon_{n\mathbf{q}}^{\sigma} + \epsilon_{n'\mathbf{q+k}}^{\sigma} - i\eta} \right). \quad (22)$$

The rational expression in the brackets complicates a direct summation over the Brillouin zone. It is more convenient to consider the representation $(\mathrm{Im}\, P)_{IJ}(\mathbf{k}, \omega)$ of the imaginary part $\mathrm{Im}\, P(\mathbf{r}, \mathbf{r}'; \omega)$ first, which is obtained by replacing expressions of the form $1/(a \pm i\eta)$ by $\mp \pi \delta(a)$. This simplifies the BZ summation significantly. Afterwards a Hilbert transformation yields the full polarization matrix $P_{IJ}(\mathbf{k}, \omega)$, where the frequency argument may be complex. In particular, this allows an evaluation on the imaginary-frequency axis, where the frequency-dependent quantities show a smooth behavior and can therefore be sampled and interpolated with few frequency points. As the bracket in Eq. (22) is real for frequencies on the imaginary axis, the corresponding matrix $P_{IJ}(\mathbf{k}, i\omega)$ with $\omega \in \mathbb{R}$ becomes Hermitian; it even becomes real symmetric if the system exhibits inversion symmetry and we use a symmetrized MPB as described in Sec. III B.

In the MPB, the integral equations for the dielectric function [Eq. (9)] and the screened interaction [Eq. (10)] turn into simple matrix equations. The equations become particularly simple if we perform a basis transformation $\{M_I^{\mathbf{k}}(\mathbf{r})\} \to \{E_\mu^{\mathbf{k}}(\mathbf{r})\}$ that diagonalizes the Coulomb matrix. We note that no approximation is involved at this stage. The new normalized basis functions are necessarily orthogonal, and we do not need a biorthogonal set. In this new basis, the matrix equations become simple products,

$$\varepsilon_{\mu\nu}(\mathbf{k}, \omega) = \delta_{\mu\nu} - \sqrt{v_\mu(\mathbf{k})} P_{\mu\nu}(\mathbf{k}, \omega) \sqrt{v_\nu(\mathbf{k})}, \quad (23)$$

$$W_{\mu\nu}(\mathbf{k}, \omega) = \sqrt{v_\mu(\mathbf{k})} \varepsilon_{\mu\nu}^{-1}(\mathbf{k}, \omega) \sqrt{v_\nu(\mathbf{k})} \quad (24)$$

with the eigenvalues $v_\mu(\mathbf{k})$ of the Coulomb matrix [Eq. (21)]. Here we use a symmetrized definition of the dielectric matrix $\varepsilon_{\mu\nu}(\mathbf{k}, \omega)$ that is Hermitian (or real symmetric in case of inversion symmetry) for imaginary frequencies and remains finite at the Γ point. It is easy to verify that the screened interaction remains unchanged by this symmetrized formulation.

In contrast to the exchange self-energy, the frequency integral in Eq. (13) cannot be replaced by a sum over residues because the positions of the poles of $W_{\mu\nu}^{\mathrm{c}}(\mathbf{k}, \omega) = W_{\mu\nu}(\mathbf{k}, \omega) - \delta_{\mu\nu} v_\mu(\mathbf{k})$ in the complex-frequency plane are unknown. Therefore, the correlation self-energy,

$$\langle \varphi_{n\mathbf{q}}^{\sigma} | \Sigma_{\mathrm{c}}^{\sigma}(\omega) | \varphi_{n\mathbf{q}}^{\sigma} \rangle = \frac{i}{2\pi} \sum_{\mathbf{k}}^{\mathrm{BZ}} \sum_{n'}^{\mathrm{all}} \sum_{\mu,\nu}^{} \langle \varphi_{n'\mathbf{q+k}}^{\sigma} | \varphi_{n\mathbf{q}}^{\sigma} E_\mu^{\mathbf{k}} \rangle$$
$$\times \langle E_\nu^{\mathbf{k}} \varphi_{n\mathbf{q}}^{\sigma} | \varphi_{n'\mathbf{q+k}}^{\sigma} \rangle$$
$$\times \int_{-\infty}^{\infty} d\omega' \frac{W_{\mu\nu}^{\mathrm{c}}(\mathbf{k}, \omega')}{\omega + \omega' - \epsilon_{n'\mathbf{q+k}}^{\sigma} + i\eta \, \mathrm{sgn}(\epsilon_{n'\mathbf{q+k}}^{\sigma})} \quad (25)$$

still contains an explicit integration over frequencies. Unfortunately, the integrand has a lot of structure along the real frequency axis, which makes a direct evaluation difficult. There are two methods that avoid the integration over real frequencies and use the imaginary axis instead: analytic continuation[29] and contour integration.[30] The former allows a faster and easier implementation but contains a badly controlled fitting procedure, which can be tested with the more accurate contour-integration method. We have implemented both algorithms and find that they give similar results for the systems considered here. In the following, we hence focus exclusively on the first approach, which is based on an analytic continuation of Eq. (25) to the imaginary-frequency axis,

$$\langle \varphi_{n\mathbf{q}}^{\sigma} | \Sigma_{\mathrm{c}}^{\sigma}(i\omega) | \varphi_{n\mathbf{q}}^{\sigma} \rangle = -\frac{1}{2\pi} \sum_{\mathbf{k}}^{\mathrm{BZ}} \sum_{n'}^{\mathrm{all}} \sum_{\mu,\nu}^{} \langle \varphi_{n'\mathbf{q+k}}^{\sigma} | \varphi_{n\mathbf{q}}^{\sigma} E_\mu^{\mathbf{k}} \rangle$$
$$\times \langle E_\nu^{\mathbf{k}} \varphi_{n\mathbf{q}}^{\sigma} | \varphi_{n'\mathbf{q+k}}^{\sigma} \rangle$$
$$\times \int_{-\infty}^{\infty} d\omega' \frac{W_{\mu\nu}^{\mathrm{c}}(\mathbf{k}, i\omega')}{i\omega + i\omega' - \epsilon_{n'\mathbf{q+k}}^{\sigma}}. \quad (26)$$

The integration contour can be closed over the positive imaginary and negative real half plane in Eqs. (25) and (26), respectively, and encloses the same poles. Now the frequency integration is along the imaginary-frequency axis, where the integrand is much smoother. In practice, we use a discrete and finite mesh for the imaginary frequencies, which is dense near $\omega = 0$. A tail is fitted to the last mesh point according to the known asymptotic ω^{-2} behavior of the screened interaction. Between the mesh points, we interpolate $W_{\mu\nu}^{\mathrm{c}}(\mathbf{k}, \omega(\lambda))$ with cubic splines, where $\omega(\lambda) = \lambda/(1-\lambda)$

maps the interval $[0,1[$ to $[0,\infty[$. This allows a stepwise analytic integration. With this procedure only a small number of mesh points is needed, typically around 10.

Once the correlation self-energy is calculated on the discrete imaginary-frequency mesh, we analytically continue it to the whole complex plane by fitting the model function,

$$f(\omega) = \sum_{p=1}^{N_p} \frac{a_p}{\omega - \omega_p} \quad \text{for } \text{Re } \omega \geq 0 \quad (27)$$

with complex fit parameters a_p and ω_p. Due to the location of the poles of the correlation self-energy in the complex plane—above the real axis for $\text{Re } \omega < 0$ and below the real axis for $\text{Re } \omega > 0$—one must analytically continue from the positive imaginary axis to the positive real axis. For symmetry reasons one then obtains

$$f(\omega) = \sum_{p=1}^{N_p} \frac{a_p^*}{\omega - \omega_p^*} \quad \text{for } \text{Re } \omega < 0 \quad (28)$$

on the negative real axis. In principle, N_p is a convergence parameter. However, as the number of imaginary frequencies where $\langle \varphi_{n\mathbf{q}}^\sigma | \Sigma_c^\sigma(i\omega) | \varphi_{n\mathbf{q}}^\sigma \rangle$ is known is relatively small, and as the fitting procedure quickly becomes prohibitive for large numbers of fit parameters, one usually uses only few poles, e.g., $N_p=3$. After finding the parameters a_p and ω_p, the correlation self-energy $\langle \varphi_{n\mathbf{q}}^\sigma | \Sigma_c^\sigma(\omega) | \varphi_{n\mathbf{q}}^\sigma \rangle$ is approximated by the analytic function $f(\omega)$, which allows to solve the nonlinear quasiparticle equation (4) to machine precision with the standard iterative Newton method and without any additional linearization of the self-energy.

D. Brillouin-zone sampling

Both the polarization function and the self-energy are defined as products in real space. These become the convolutions [Eqs. (19), (22), and (25)] in a reciprocal-space formulation, which is better suited for infinite periodic systems because all nonlocal quantities then become block diagonal. We employ the tetrahedron method for summations over the BZ.[31]

These equations do not only contain the two Bloch vectors $\mathbf{k}$ and $\mathbf{q}$ but also their sum $\mathbf{k}+\mathbf{q}$, at which the KS wave functions and energies must be known. Therefore, we choose the set of $\mathbf{k}$ points $\mathbf{k}_{n_1 n_2 n_3} = \sum_{i=1}^{3} n_i \mathbf{b}_i / N_i$ with $n_i = 0, \ldots, N_i - 1$ and the reciprocal basis vectors $\mathbf{b}_i$. We denote the number of $\mathbf{k}$ points by $N_\mathbf{k} = N_1 N_2 N_3$. It naturally includes the point $\mathbf{k}=\mathbf{0}$, which is special because the long-range nature of the Coulomb interaction makes the Coulomb matrix $v_{IJ}(\mathbf{k})$ and also the screened interaction $W_{\mu\nu}(\mathbf{k}, \omega)$ diverge in the limit $\mathbf{k} \to \mathbf{0}$. This divergence must be taken into account in order to obtain fast convergence with respect to the $\mathbf{k}$-point sampling. We will discuss a numerically stable and efficient treatment in the next section.

E. Γ-point treatment

The exchange and correlation self-energy contributions in Eqs. (19) and (26) each contain a sum over the BZ. The interaction potentials $v_{IJ}(\mathbf{k})$ and $W_{\mu\nu}(\mathbf{k}, \omega)$ diverge in the

limit $\mathbf{k} \to \mathbf{0}$ but as this pole is only of second order ($1/k^2$), a proper three-dimensional integration over $\mathbf{k}=\mathbf{0}$ will yield a finite value.

Likewise, the calculation of the dielectric matrix [Eq. (23)] involves a product of the polarization function and the divergent Coulomb matrix. However, a closer inspection of the polarization matrix [Eq. (22)] in the basis $\{E_\mu^\mathbf{k}(\mathbf{r})\}$ shows that the head element $P_{11}(\mathbf{k}, \omega)$ and the wing elements $P_{\mu 1}(\mathbf{k}, \omega)$ and $P_{1\mu}(\mathbf{k}, \omega)$ with $\mu > 1$ are of the order k^2 and k, respectively, so that the dielectric matrix $\varepsilon(\mathbf{k}, \omega)$ remains finite but angular dependent at $\mathbf{k}=\mathbf{0}$.[32]

In any case, the divergence gives an important contribution to the self-energies and response functions and must be treated with care. There are several numerical approaches. Kotani and van Schilfgaarde[12] replaced the Γ point by three additional points $\mathbf{k}_0$ nearby, the so-called offset Γ points. These might be reduced by symmetry, e.g., to a single point in the case of cubic symmetry. However, because of the summations in Eqs. (19), (22), and (26), each additional point $\mathbf{k}_0$ requires a complete auxiliary mesh $\{\mathbf{k}_0 + \mathbf{q}, \mathbf{q} \in \text{BZ}\}$ on which the KS Hamiltonian must be diagonalized and the resulting wave functions and energies must be stored. This at least doubles the $\mathbf{k}$-point set, thus increasing the numerical cost in terms of computation time and memory demand. In another approach, Ku and Eguiluz[10] as well as Puschnig and Ambrosch-Draxl[19] used a plane-wave basis for the Coulomb potential and related propagators and thereby departed from a complete all-electron description because plane waves are too inflexible to resolve the rapid variations in the wave functions close to the atomic cores without a prohibitively large basis set.

Here we present a scheme that does not require additional $\mathbf{k}$ points or projections onto plane waves. It thus combines the accuracy of an all-electron approach with the numerical efficiency of a minimal $\mathbf{k}$-point set. In the following, we present the algorithm for the two self-energy contributions and the dielectric matrix.

1. Exchange self-energy

If the $\mathbf{k}$-point summation in Eq. (19) is replaced by an integral, we can smoothly integrate over the divergence of $v_{IJ}(\mathbf{k})$ and obtain a finite value. To this end, we formally consider the Fourier transform

$$v_{\mathbf{GG}'}(\mathbf{k}) = \frac{1}{V} \int \frac{e^{-i(\mathbf{k}+\mathbf{G})\cdot\mathbf{r}} e^{i(\mathbf{k}+\mathbf{G}')\cdot\mathbf{r}'}}{|\mathbf{r} - \mathbf{r}'|} d^3r d^3r' = \frac{4\pi}{k^2} \delta_{\mathbf{G0}} \delta_{\mathbf{G}'0}$$
$$+ v_{\mathbf{GG}'}'(\mathbf{k}) \quad (29)$$

with the nondivergent and infinitely large matrix $v_{\mathbf{GG}'}'(\mathbf{k}) = (1-\delta_{\mathbf{G0}}) \delta_{\mathbf{GG}'} 4\pi/|\mathbf{k}+\mathbf{G}|^2$. In a previous publication,[20] we found an analogous exact decomposition of the Coulomb matrix [Eq. (21)] into the same divergent term and a nondivergent remainder $v_{IJ}'(\mathbf{0})$. Thus no projection onto plane waves is necessary, and we retain the full accuracy of our all-electron formulation. Replacing $v_{\mathbf{GG}}'(\mathbf{0})$ by $v_{IJ}'(\mathbf{0})$ and inserting Eq. (29) into Eq. (19) leads to contributions from the divergent term

$$\langle\varphi_{n\mathbf{q}}^\sigma|\Sigma_{\mathrm{x}}^\sigma|\varphi_{n\mathbf{q}}^\sigma\rangle_{\mathrm{div}} = -\frac{4\pi f_{n\mathbf{q}}^\sigma}{V}\left(\frac{V}{8\pi^3}\int_{\mathrm{BZ}}\frac{1}{k^2}d^3k - \sum_{\mathbf{k}\neq\mathbf{0}}^{\mathrm{BZ}}\frac{1}{k^2}\right)$$

$$(30)$$

with the occupation numbers $f_{n\mathbf{q}}^\sigma$ and from the nondivergent term

$$\langle\varphi_{n\mathbf{q}}^\sigma|\Sigma_{\mathrm{x}}^\sigma|\varphi_{n\mathbf{q}}^\sigma\rangle_{\mathrm{ndiv}} = -\sum_{\mathbf{k}}^{\mathrm{BZ}}\sum_{n'}^{\mathrm{occ}}\sum_{I,J}v_{IJ}(\mathbf{k})\langle\tilde{M}_J^{\mathbf{k}}\varphi_{n\mathbf{q}}^\sigma|\varphi_{n'\mathbf{q}+\mathbf{k}}^\sigma\rangle$$

$$\times\langle\varphi_{n'\mathbf{q}+\mathbf{k}}^\sigma|\varphi_{n\mathbf{q}}^\sigma\tilde{M}_I^{\mathbf{k}}\rangle,\qquad(31)$$

where we have set $v_{IJ}'(\mathbf{0})\to v_{IJ}(\mathbf{0})$ for simplicity. The divergence of the Coulomb matrix is restricted to the first term of Eq. (29), and the corresponding eigenfunction is $e^{i\mathbf{k}\cdot\mathbf{r}}/\sqrt{V}$, whose $\mathbf{k}\to\mathbf{0}$ limit, a constant function, can be represented exactly by the MPB. The products of $1/k^2$ with higher-order terms of the projections $\langle e^{i\mathbf{k}\cdot\mathbf{r}}\varphi_{n\mathbf{q}}^\sigma|\varphi_{n'\mathbf{q}+\mathbf{k}}^\sigma\rangle/\sqrt{V}$ can be of zeroth order and then lead to additional contributions to Eq. (31) for $\mathbf{k}=\mathbf{0}$. Therefore, the projections must be expanded with the help of $\mathbf{k}\cdot\mathbf{p}$ perturbation theory. We have found that these corrections improve the $\mathbf{k}$-point convergence significantly in some cases while in others—especially for small band-gap semiconductors like GaAs—they worsen the convergence. The behavior also depends on the particular electronic state $|\varphi_{n\mathbf{q}}^\sigma\rangle$. For simplicity, we defer an in-depth discussion to a later publication.

In order to be able to integrate analytically, we extend the BZ integral in Eq. (30) to the whole reciprocal space by replacing $1/k^2$ with

$$F(\mathbf{k}) = \sum_{\mathbf{G}}\frac{e^{-\beta|\mathbf{k}+\mathbf{G}|^2}}{|\mathbf{k}+\mathbf{G}|^2}.\qquad(32)$$

Note that $F(\mathbf{k})$ diverges at every reciprocal-lattice vector $\mathbf{G}$. The exponential function was included to ensure the convergence of the sum everywhere else. This function is formally identical to the one used by Massidda *et al.* in Ref. 33. However, these authors define β as a parameter depending on the BZ size. Instead, we choose β to be as small as possible (while still allowing a sufficiently fast converging sum over $\mathbf{G}$), independently of the BZ. First, this ensures that supercell calculations of the same system yield identical values. Second, zero-order terms arising from products of the exponential function with $1/k^2$ are small and can be neglected. After replacing $1/k^2$ with $F(\mathbf{k})$ and extending the integral and summation over the whole reciprocal space we obtain

$$\langle\varphi_{n\mathbf{q}}^\sigma|\Sigma_{\mathrm{x}}^\sigma|\varphi_{n\mathbf{q}}^\sigma\rangle_{\mathrm{div}}$$
$$= -4\pi f_{n\mathbf{q}}^\sigma\left(\frac{1}{8\pi^3}\int\frac{e^{-\beta q^2}}{q^2}d^3q - \frac{1}{\Omega N_{\mathbf{k}}}\sum_{0<|\mathbf{q}|}\frac{e^{-\beta q^2}}{q^2}\right),$$

$$(33)$$

where the sum runs over all vectors $\mathbf{q}=\mathbf{k}+\mathbf{G}\neq\mathbf{0}$ and Ω is the unit-cell volume. As both terms diverge for $\beta\to0$, we introduce a cutoff radius q_0 and finally obtain

$$\langle\varphi_{n\mathbf{q}}^\sigma|\Sigma_{\mathrm{x}}^\sigma|\varphi_{n\mathbf{q}}^\sigma\rangle_{\mathrm{div}}$$
$$= -f_{n\mathbf{q}}^\sigma\left[\frac{1}{\sqrt{\pi\beta}}\mathrm{erf}(\sqrt{\beta}q_0) - \frac{4\pi}{\Omega N_{\mathbf{k}}}\sum_{0<|\mathbf{q}|<q_0}\frac{e^{-\beta q^2}}{q^2}\right].$$

$$(34)$$

We get rid of q_0 as a convergence parameter by choosing $e^{-\beta q_0^2}=\beta$ as a cutoff criterion for the summation. In practice, we find that $\beta=0.005$ is typically small enough.

2. Response functions

The treatment of the polarization and dielectric function in the limit $\mathbf{k}\to\mathbf{0}$ is simplified considerably by the basis transformation $\{M_I^{\mathbf{k}}(\mathbf{r})\}\to\{E_\mu^{\mathbf{k}}(\mathbf{r})\}$ introduced in Sec. III C because it confines the divergence of the Coulomb matrix to a single eigenvalue $v_1(\mathbf{k})\sim4\pi/k^2$ (Ref. 20). The corresponding eigenfunction $E_1^{\mathbf{k}}(\mathbf{r})\sim e^{i\mathbf{k}\cdot\mathbf{r}}/\sqrt{V}$ is known analytically.

Let us consider the projection [Eq. (20)], where the MPB function is replaced by this eigenfunction. Because of the orthogonality of the wave functions, we have $\langle e^{i\mathbf{k}\cdot\mathbf{r}}\varphi_{n\mathbf{q}}^\sigma|\varphi_{n'\mathbf{q}+\mathbf{k}}^\sigma\rangle\sim\delta_{nn'}$ in the limit $\mathbf{k}\to\mathbf{0}$. For the moment, we restrict ourselves to the case of semiconductors and insulators where the band indices n for occupied and n' for unoccupied states always differ such that in leading order $\langle e^{i\mathbf{k}\cdot\mathbf{r}}\varphi_{n\mathbf{q}}^\sigma|\varphi_{n'\mathbf{q}+\mathbf{k}}^\sigma\rangle\sim k$. The linear order in k exactly cancels the singularity of the Coulomb matrix in the dielectric function [Eq. (23)] and can be calculated with $\mathbf{k}\cdot\mathbf{p}$ perturbation theory,[32] which allows a full treatment of the divergence and the dielectric anisotropy at $\mathbf{k}=\mathbf{0}$.[34] In this way, the matrices decompose into head, wings, and body as in a simple plane-wave basis set. Still, the all-electron accuracy is fully retained and no projection onto plane waves is necessary.

For the sake of completeness here, we give the exact expressions for the polarization function and the screened interaction, taking into account the full anisotropy. From $\mathbf{k}\cdot\mathbf{p}$ perturbation theory, one obtains the form

$$P_{\mu\nu}(\mathbf{k},i\omega)\sim\begin{pmatrix}\mathbf{e}_{\mathbf{k}}^{\mathrm{T}}\mathbf{H}(\omega)\mathbf{e}_{\mathbf{k}}k^2 & \mathbf{e}_{\mathbf{k}}^{\mathrm{T}}\mathbf{s}_2(\omega)k & \cdots & \mathbf{e}_{\mathbf{k}}^{\mathrm{T}}\mathbf{s}_n(\omega)k\\ \mathbf{e}_{\mathbf{k}}^{\mathrm{T}}\mathbf{s}_2^*(\omega)k & \tilde{P}_{22}(\omega) & \cdots & \tilde{P}_{2n}(\omega)\\ \vdots & \vdots & \ddots & \vdots\\ \mathbf{e}_{\mathbf{k}}^{\mathrm{T}}\mathbf{s}_n^*(\omega)k & \tilde{P}_{n2}(\omega) & \cdots & \tilde{P}_{nn}(\omega)\end{pmatrix}$$

$$(35)$$

for the polarization function in the limit $\mathbf{k}\to\mathbf{0}$. Here $\mathbf{H}(\omega)$ is a 3×3 matrix, $\mathbf{s}_\mu(\omega)$ are three-dimensional vectors, and the matrix elements $\tilde{P}_{\mu\nu}(\omega)$ are finite. We note that for frequency arguments that are not purely imaginary the matrix $P_{\mu\nu}(\mathbf{k},\omega)$ is not Hermitian; in particular, the horizontal and vertical wings are then not simply the complex conjugates of one another. Otherwise, the formalism is very similar to the one given here. The corresponding screened interaction becomes

$$W_{\mu\nu}(\mathbf{k}, i\omega) \sim \begin{pmatrix} 0 & 0 & \cdots & 0 \\ 0 & \widetilde{W}_{22}(\omega) & \cdots & \widetilde{W}_{2n}(\omega) \\ \vdots & \vdots & \ddots & \vdots \\ 0 & \widetilde{W}_{n2}(\omega) & \cdots & \widetilde{W}_{nn}(\omega) \end{pmatrix} + \frac{1}{\mathbf{e}_{\mathbf{k}}^{\mathrm{T}}\mathbf{L}(\omega)\mathbf{e}_{\mathbf{k}}} \begin{pmatrix} 4\pi/k^2 & \mathbf{e}_{\mathbf{k}}^{\mathrm{T}}\mathbf{w}_2(\omega)/k & \cdots & \mathbf{e}_{\mathbf{k}}^{\mathrm{T}}\mathbf{w}_n(\omega)/k \\ \mathbf{e}_{\mathbf{k}}^{\mathrm{T}}\mathbf{w}_2^*(\omega)/k & |\mathbf{e}_{\mathbf{k}}^{\mathrm{T}}\mathbf{w}_2(\omega)|^2 & \cdots & [\mathbf{e}_{\mathbf{k}}^{\mathrm{T}}\mathbf{w}_2^*(\omega)][\mathbf{e}_{\mathbf{k}}^{\mathrm{T}}\mathbf{w}_n(\omega)] \\ \vdots & \vdots & \ddots & \vdots \\ \mathbf{e}_{\mathbf{k}}^{\mathrm{T}}\mathbf{w}_n^*(\omega)/k & [\mathbf{e}_{\mathbf{k}}^{\mathrm{T}}\mathbf{w}_n^*(\omega)][\mathbf{e}_{\mathbf{k}}^{\mathrm{T}}\mathbf{w}_2(\omega)] & \cdots & |\mathbf{e}_{\mathbf{k}}^{\mathrm{T}}\mathbf{w}_n(\omega)|^2 \end{pmatrix} \tag{36}$$

with the finite matrix elements

$$\widetilde{W}_{\mu\nu}(\omega) = \sqrt{v_\mu(\mathbf{0})}\,\widetilde{\varepsilon}_{\mu\nu}^{-1}(\omega)\sqrt{v_\nu(\mathbf{0})}, \tag{37}$$

$$\widetilde{\varepsilon}_{\mu\nu}(\omega) = \delta_{\mu\nu} - \sqrt{v_\mu(\mathbf{0})}\,\widetilde{P}_{\mu\nu}(\omega)\sqrt{v_\nu(\mathbf{0})}, \tag{38}$$

where $\mu, \nu \geq 2$. The divergent and, in general, angular-dependent second term derives from the head and wing elements of Eq. (35) with

$$\mathbf{w}_\mu(\omega) = \sqrt{4\pi}\sum_{\nu \geq 2} \widetilde{\varepsilon}_{\mu\nu}^{-1}(\omega)\mathbf{s}_\nu(\omega)\sqrt{v_\nu(\mathbf{0})} \tag{39}$$

and

$$\mathbf{L}(\omega) = \mathbf{1} - 4\pi\mathbf{H}(\omega) - \sqrt{4\pi}\sum_{\mu \geq 2} \mathbf{s}_\mu(\omega)\mathbf{w}_\mu^{\mathrm{T}}(\omega)\sqrt{v_\mu(\mathbf{0})}. \tag{40}$$

Let us now turn to the case of a metallic system, where in addition to the interband transitions with $n \neq n'$, there is a contribution from intraband transitions across the Fermi surface. These transitions occur within one electron band, i.e., $n = n'$, in which case the projection above becomes unity in the limit $\mathbf{k} \to \mathbf{0}$. However, it can be shown[35] that the expression in the brackets of Eq. (22) will then be of linear order in $\mathbf{k}$ and that we obtain a contribution only for the head element of the polarization matrix, the so-called Drude term

$$P_{11}^{\mathrm{D}}(\mathbf{k}, i\omega) \sim -\frac{k^2}{4\pi}\frac{\omega_{\mathrm{pl}}^2}{\omega(\omega + i\eta)}, \tag{41}$$

where ω_{pl} is the plasma frequency obtained by an integration over the Fermi surface. The Drude term gives rise to a contribution $\omega_{\mathrm{pl}}^2/[\omega(\omega + i\eta)]$ for the head element of the dielectric matrix [Eq. (23)], which will mix with all other elements in the inversion for the screened interaction [Eq. (24)]. However, we find that $W_{11}^{\mathrm{c}}(\mathbf{k}, \omega)$ is dominated by the *bare* Drude term

$$W_{11}^{\mathrm{c,D}}(\mathbf{k}, i\omega) \sim -\frac{4\pi}{k^2}\frac{\omega_{\mathrm{pl}}^2}{\omega^2 + \omega_{\mathrm{pl}}^2} \tag{42}$$

in the limit $\mathbf{k} \to \mathbf{0}$. As this expression can be convoluted with the Green function in Eq. (26) analytically, we subtract it from the head element and treat the remainder $W_{11}^{\mathrm{c}}(\mathbf{k}, i\omega) - W_{11}^{\mathrm{c,D}}(\mathbf{k}, i\omega)|_{\mathbf{k} \to \mathbf{0}}$ numerically. The treatment of the $1/k^2$ divergence is explained in the next section.

3. Correlation self-energy

The BZ summation over the $1/k^2$ divergence in the correlation self-energy [Eq. (25)] can be treated with the same procedure as outlined in Sec. III E 1 for the exchange self-energy. However, in this case, there are additional $1/k$ terms, and all divergent terms exhibit an additional angular dependence.

As a first step we describe this angular dependence with the help of spherical harmonics. For example, for the head element we must find the coefficients $K_{(2l)m}(\omega)$ in

$$\frac{4\pi}{\mathbf{e}_{\mathbf{k}}^{\mathrm{T}}\mathbf{L}(\omega)\mathbf{e}_{\mathbf{k}}} = \sum_{l=0}^{\infty}\sum_{m=-2l}^{2l} K_{(2l)m}(\omega)Y_{(2l)m}(\mathbf{e}_{\mathbf{k}}). \tag{43}$$

If we multiply with the denominator $\mathbf{e}_{\mathbf{k}}^{\mathrm{T}}\mathbf{L}(\omega)\mathbf{e}_{\mathbf{k}} = \sum_{l=0}^{1}\sum_{m=-l}^{l} L_{(2l)m}(\omega)Y_{(2l)m}^*(\mathbf{e}_{\mathbf{k}})$, use the Gaunt coefficients and the orthogonality of spherical harmonics, we obtain an infinite system of linear equations, from which the coefficients $K_{(2l)m}(\omega)$ can be deduced. The corresponding expansions for the wing,

$$\frac{\mathbf{e}_{\mathbf{k}}^{\mathrm{T}}\mathbf{w}_\mu(\omega)}{\mathbf{e}_{\mathbf{k}}^{\mathrm{T}}\mathbf{L}(\omega)\mathbf{e}_{\mathbf{k}}} = \sum_{l=0}^{\infty}\sum_{m=-(2l+1)}^{2l+1} K_{\mu,(2l+1)m}(\omega)Y_{(2l+1)m}(\mathbf{e}_{\mathbf{k}}) \tag{44}$$

and body matrix elements can be calculated in a similar way. Finally, subtraction of $\delta_{\mu\nu}v_\mu(\mathbf{0})$ with $v_1(\mathbf{0}) \sim 4\pi/k^2$ yields the expansions for the head and body of W^{c}. Then $K_{(2l)m}^{\mathrm{c}}(\omega) = K_{(2l)m}(\omega) - (4\pi)^{3/2}\delta_{l0}$ and $\widetilde{W}_{\mu\nu}^{\mathrm{c}}(\omega) = \widetilde{W}_{\mu\nu}(\omega) - \delta_{\mu\nu}v_\mu(\mathbf{0})$ replace $K_{(2l)m}(\omega)$ and $\widetilde{W}_{\mu\nu}(\omega)$, respectively.

The body matrix elements of the second term in Eq. (36) are angular dependent but finite. Then all terms with $l > 0$ integrate to zero, and we retain only the constant term $l = 0$, which we simply add to $\widetilde{W}_{\mu\nu}^{\mathrm{c}}$. The head (wing) elements diverge with a factor $k^{-2}(k^{-1})$. As in Sec. III E 1, multiplication with higher orders of the projections and the term $1/(i\omega + i\omega' - \epsilon_{n'\mathbf{q}+\mathbf{k}}^\sigma)$ leads to terms of zeroth order in $\mathbf{k}$. Again we do not discuss these terms explicitly, as they improve the results only in some cases, while in others, they can lead to numerical problems. This can be attributed to the energy denominators of $\mathbf{k} \cdot \mathbf{p}$ perturbation theory, which is used to compute the higher-order terms.

The head element exhibits a $1/k^2$ divergence, which can be treated in the same way as in Sec. III E 1. We obtain a contribution

$$\langle \varphi_{n\mathbf{q}}^{\sigma}|\Sigma_{\mathrm{c}}^{\sigma}(i\omega)|\varphi_{n\mathbf{q}}^{\sigma}\rangle_{\mathrm{div}} = -\frac{1}{4\pi^{3/2}V}\left(\frac{V}{8\pi^3}\int_{\mathrm{BZ}}\frac{1}{k^2}d^3k - \sum_{\mathbf{k}\neq\mathbf{0}}^{\mathrm{BZ}}\frac{1}{k^2}\right)$$

$$\times \int_{-\infty}^{\infty}\frac{K_{00}^{\mathrm{c}}(\omega')}{i\omega + i\omega' - \epsilon_{n\mathbf{q}}^{\sigma}}d\omega', \qquad (45)$$

where the frequency integration is performed as described in Sec. III C. All other elements $K_{(2l)m}^{\mathrm{c}}(\omega)$ as well as the divergent wing elements of Eq. (36) need not be taken into account, as their angular parts integrate to zero. However, we note that there is a finite contribution of these elements from multiplications with higher-order terms of the other quantities—a contribution that we neglect here for simplicity, as previously mentioned.

F. Optimization of the MPB

If we assume that the eigenvalues $v_\mu(\mathbf{k})$ are ordered according to decreasing size, then matrix elements $\varepsilon_{\mu\nu}(\mathbf{k},\omega)$ and $W_{\mu\nu}(\mathbf{k},\omega)$ with large indices will be relatively small, cf. Eqs. (23) and (24). We may then introduce a threshold value $v_{\min}$ for the eigenvalues and only retain the functions $E_\mu^{\mathbf{k}}(\mathbf{r})$ with $v_\mu(\mathbf{k})\geq v_{\min}$. As the eigenvalue $v_\mu(\mathbf{k})$ can be viewed as a measure for the importance of the corresponding function $E_\mu^{\mathbf{k}}(\mathbf{r})$ in $v(\mathbf{r})$, we restrict ourselves to the dominant part of the electron-electron interaction in this way. The removal of basis functions with small eigenvalues can be viewed as an optimization step of the MPB because it reduces the matrix sizes and hence the computational cost considerably without compromising the accuracy, as we show in Sec. IV below. We there also demonstrate that the results converge reasonably fast with respect to the threshold parameter $v_{\min}$. Note that with $v_{\min}=0$, the full accuracy of the MPB is restored. In our implementation, this optimization of the MPB only affects the correlation self-energy while we always calculate the exchange self-energy with the full MPB.

G. Use of symmetry

The evaluation of Eqs. (19), (22), and (26) takes considerable computation time, which can be reduced substantially by exploiting spatial and time-reversal symmetries of the system, the latter in case of a system without inversion symmetry. Allowed symmetry operations are those that leave the Hamiltonian invariant. With these operations, the set of $\mathbf{k}$ vectors decomposes into groups of equivalent vectors, which are equivalent in the sense that all elements of the group can be generated by applying the symmetry operations to an arbitrary representative of the group elements. As a consequence, any physical quantity defined for the representative $\mathbf{k}$ vector can be mapped to any other vector of the group by a suitable symmetry operation. This reduces the full BZ sampling to the smaller set of representative vectors, which form the irreducible BZ (IBZ).

We may thus restrict $P_{IJ}(\mathbf{k},\omega)$ to $\mathbf{k}\in\mathrm{IBZ}$. The summation over $\mathbf{q}$ points in Eq. (22), on the other hand, cannot be confined in the same way because the terms to be summed also depend on $\mathbf{k}$ (and $\mathbf{q}+\mathbf{k}$). However, we can restrict the $\mathbf{q}$ vectors to an *extended* IBZ [EIBZ($\mathbf{k}$)] that is defined in the

same way as the IBZ above but with the subset of symmetry operations that leave the given $\mathbf{k}$ vector invariant.

Let us define the complete set of N_A symmetry operations by

$$S_A = \{\hat{\mathcal{A}}_i = (\mathbf{A}_i,\mathbf{a}_i,\alpha_i)|i = 1, \ldots, N_A\}, \qquad (46)$$

where $\mathbf{A}_i$ and $\mathbf{a}_i$ denote the 3×3 rotation (or rotoinversion) matrix and a translation vector (which is nonzero for nonsymmorphic operations), respectively, and α_i equals $-1(+1)$ for operations with (without) time reversal. The action of $\hat{A}_i$ on a spatial vector $\mathbf{r}$, a momentum vector $\mathbf{k}\in\mathrm{BZ}$, and a function $f(\mathbf{r})$ is declared by

$$\hat{A}_i\mathbf{r} = \mathbf{A}_i\mathbf{r} + \mathbf{a}_i, \qquad (47)$$

$$\hat{A}_i\mathbf{k} = \alpha_i\mathbf{A}_i\mathbf{k} + \overline{\mathbf{G}}, \qquad (48)$$

$$\hat{A}_i f(\mathbf{r}) = \begin{cases} f[\mathbf{A}^{-1}(\mathbf{r} - \mathbf{a}_i)] & \text{for } \alpha_i = 1 \\ f^*[\mathbf{A}^{-1}(\mathbf{r} - \mathbf{a}_i)] & \text{for } \alpha_i = -1, \end{cases} \qquad (49)$$

where the reciprocal-lattice vector $\overline{\mathbf{G}}$ folds $\alpha_i\mathbf{A}_i\mathbf{k}$ back into the BZ. Furthermore, we define the subset

$$S_A^{\mathbf{k}} = \{\hat{A}_i^{\mathbf{k}}|i = 1, \ldots, N_A^{\mathbf{k}};\hat{A}_i^{\mathbf{k}}\mathbf{k} = \mathbf{k}\} \in S_A \qquad (50)$$

that generates the EIBZ($\mathbf{k}$).

Now we reformulate Eq. (22) using the definition of the EIBZ($\mathbf{k}$) and that $\hat{A}_i\varphi_{n\mathbf{q}}^{\sigma}(\mathbf{r})$ is a valid wave function with momentum vector $\hat{A}_i\mathbf{q}$,

$$P_{IJ}(\mathbf{k},\omega) = \sum_{i=1}^{N_A^{\mathbf{k}}}\sum_{\sigma}\sum_{\mathbf{q}}^{\mathrm{EIBZ}(\mathbf{k})}\frac{N_{\mathbf{q}}^{\mathbf{k}}}{N_A^{\mathbf{k}}}\sum_{n}^{\mathrm{occ}}\sum_{n'}^{\mathrm{unocc}}\langle \tilde{M}_I^{\mathbf{k}}\hat{A}_i^{\mathbf{k}^{-1}}\varphi_{n\mathbf{q}}^{\sigma}|\hat{A}_i^{\mathbf{k}^{-1}}\varphi_{n'\mathbf{q}+\mathbf{k}}^{\sigma}\rangle$$

$$\times \langle \hat{A}_i^{\mathbf{k}^{-1}}\varphi_{n'\mathbf{q}+\mathbf{k}}^{\sigma}|\hat{A}_i^{\mathbf{k}^{-1}}\varphi_{n\mathbf{q}}^{\sigma}\tilde{M}_J^{\mathbf{k}}\rangle(\ldots)$$

$$= \sum_{i=1}^{N_A^{\mathbf{k}}}\sum_{\sigma}\sum_{\mathbf{q}}^{\mathrm{EIBZ}(\mathbf{k})}\frac{N_{\mathbf{q}}^{\mathbf{k}}}{N_A^{\mathbf{k}}}\sum_{n}^{\mathrm{occ}}\sum_{n'}^{\mathrm{unocc}}\hat{T}_{\alpha_i}[\langle \hat{A}_i^{\mathbf{k}}\tilde{M}_I^{\mathbf{k}}\varphi_{n\mathbf{q}}^{\sigma}|\varphi_{n'\mathbf{q}+\mathbf{k}}^{\sigma}\rangle$$

$$\times \langle \varphi_{n'\mathbf{q}+\mathbf{k}}^{\sigma}|\varphi_{n\mathbf{q}}^{\sigma}\hat{A}_i^{\mathbf{k}}\tilde{M}_J^{\mathbf{k}}\rangle](\ldots), \qquad (51)$$

where $N_{\mathbf{q}}^{\mathbf{k}}$ is the number of equivalent $\mathbf{q}$ vectors with respect to $S_A^{\mathbf{k}}$, $\hat{T}_1$ the identity, and $\hat{T}_{-1}$ the transpose operator $\hat{T}_{-1}B_{IJ}=B_{JI}$. From the definition of the MPB, it is clear that the application of an arbitrary symmetry operation $\hat{A}_i^{\mathbf{k}}\in S_A^{\mathbf{k}}$ to any $M_I^{\mathbf{k}}(\mathbf{r})$ can be written as a linear combination of the basis functions $M_J^{\mathbf{k}}(\mathbf{r})$, such that the sum over the symmetry operations in Eq. (51) can be performed at the very end after summing over the bands, the EIBZ($\mathbf{k}$), and the spins. We note that this is also possible with the set $\{E_\mu^{\mathbf{k}}(\mathbf{r})\}$ instead of $\{M_I^{\mathbf{k}}(\mathbf{r})\}$.

In a similar way, we can accelerate the evaluation of the expectation values of $\Sigma_{\mathrm{x}}^{\sigma}$ and $\Sigma_{\mathrm{c}}^{\sigma}(\omega)$. To this end, we write Eqs. (19) and (26) in a common general form with a function $f(\mathbf{r},\mathbf{r}')$, which fulfills all symmetry properties of the system. By confining the summation over $\mathbf{k}$ points to the EIBZ($\mathbf{q}$) and summing over the symmetry operations we obtain

$$
\begin{aligned}
\langle\varphi_{n\mathbf{q}}^{\sigma}|\Sigma^{\sigma}|\varphi_{n\mathbf{q}}^{\sigma}\rangle &= \sum_{\mathbf{k}}^{\mathrm{BZ}}\sum_{n'}\int\int d^3r\,d^3r'\,\varphi_{n\mathbf{q}}^{\sigma*}(\mathbf{r})\varphi_{n'\mathbf{k}}^{\sigma}(\mathbf{r})\varphi_{n'\mathbf{k}}^{\sigma*}(\mathbf{r}')\varphi_{n\mathbf{q}}^{\sigma}(\mathbf{r}')f(\mathbf{r},\mathbf{r}') \\
&= \sum_{i=1}^{N_A^{\mathbf{q}}}\sum_{\mathbf{k}}^{\mathrm{EIBZ}(\mathbf{q})}\frac{N_{\mathbf{k}}^{\mathbf{q}}}{N_A^{\mathbf{q}}}\sum_{n'}\int\int d^3r\,d^3r'\,\varphi_{n\mathbf{q}}^{\sigma*}(\mathbf{r})[\hat{A}_i^{\mathbf{q}^{-1}}\varphi_{n'\mathbf{k}}^{\sigma}(\mathbf{r})][\hat{A}_i^{\mathbf{q}^{-1}}\varphi_{n'\mathbf{k}}^{\sigma*}(\mathbf{r}')]\varphi_{n\mathbf{q}}^{\sigma}(\mathbf{r}')f(\mathbf{r},\mathbf{r}') \\
&= \sum_{i=1}^{N_A^{\mathbf{q}}}\sum_{\mathbf{k}}^{\mathrm{EIBZ}(\mathbf{q})}\frac{N_{\mathbf{k}}^{\mathbf{q}}}{N_A^{\mathbf{q}}}\sum_{n'}\int\int d^3r\,d^3r'\,[\hat{A}_i^{\mathbf{q}}\varphi_{n\mathbf{q}}^{\sigma*}(\mathbf{r})]\varphi_{n'\mathbf{k}}^{\sigma}(\mathbf{r})\varphi_{n'\mathbf{k}}^{\sigma*}(\mathbf{r}')[\hat{A}_i^{\mathbf{q}}\varphi_{n\mathbf{q}}^{\sigma}(\mathbf{r}')]f(\mathbf{r},\mathbf{r}') \\
&= \sum_{\mathbf{k}}^{\mathrm{EIBZ}(\mathbf{q})}\frac{N_{\mathbf{k}}^{\mathbf{q}}}{N_A^{\mathbf{q}}}\sum_{m}\sum_{m'}\left(\sum_{i=1}^{N_A^{\mathbf{q}}}A_{i,mn\mathbf{q}}^{\sigma*}A_{i,m'n\mathbf{q}}^{\sigma}\right)\sum_{n'}\int\int d^3r\,d^3r'\,\varphi_{m\mathbf{q}}^{\sigma*}(\mathbf{r})\varphi_{n'\mathbf{k}}^{\sigma}(\mathbf{r})\varphi_{n'\mathbf{k}}^{\sigma*}(\mathbf{r}')\varphi_{m'\mathbf{q}}^{\sigma}(\mathbf{r}')f(\mathbf{r},\mathbf{r}'),
\end{aligned} \tag{52}
$$

where we have restricted ourselves for simplicity to symmetry operations without time reversal. $A_{i,mn\mathbf{q}}^{\sigma}=\langle\varphi_{m\mathbf{q}}^{\sigma}|\hat{A}_i^{\mathbf{q}}|\varphi_{n\mathbf{q}}^{\sigma}\rangle$ is the matrix representation of $\hat{A}_i^{\mathbf{q}}$ in terms of the wave functions. As $\hat{A}_i^{\mathbf{q}}$ commutes with the Hamiltonian, the element $A_{i,mn\mathbf{q}}^{\sigma}$ can only be nonzero if the corresponding energies $\epsilon_{m\mathbf{q}}^{\sigma}$ and $\epsilon_{n\mathbf{q}}^{\sigma}$ are identical. Let us assume that $\varphi_{m\mathbf{q}}^{\sigma}$ and $\varphi_{n\mathbf{q}}^{\sigma}$ lie in the eigenspace formed by $\varphi_{\nu\mathbf{q}}^{\sigma}$ with $n_1\le\nu\le n_2$. By construction $A_{i,mn\mathbf{q}}^{\sigma}$ is then an irreducible representation, and we may apply the great orthogonality theorem of group theory,[36]

$$
\sum_{i=1}^{N_A^{\mathbf{q}}}A_{i,mn\mathbf{q}}^{\sigma*}A_{i,m'n\mathbf{q}}^{\sigma}=\frac{N_A^{\mathbf{q}}}{n_2-n_1+1}\delta_{mm'}, \tag{53}
$$

which finally yields

$$
\langle\varphi_{n\mathbf{q}}^{\sigma}|\Sigma^{\sigma}|\varphi_{n\mathbf{q}}^{\sigma}\rangle = \sum_{\mathbf{k}}^{\mathrm{EIBZ}(\mathbf{q})}\frac{N_{\mathbf{k}}^{\mathbf{q}}}{n_2-n_1+1}\sum_{m=n_1}^{n_2}\sum_{n'}\int\int d^3r\,d^3r' \\
\times\varphi_{m\mathbf{q}}^{\sigma*}(\mathbf{r})\varphi_{n'\mathbf{k}}^{\sigma}(\mathbf{r})\varphi_{n'\mathbf{k}}^{\sigma*}(\mathbf{r}')\varphi_{m\mathbf{q}}^{\sigma}(\mathbf{r}')f(\mathbf{r},\mathbf{r}'). \tag{54}
$$

The $\mathbf{k}$-point sum is thus reduced to the EIBZ($\mathbf{q}$) but we have to average over the degenerate states $n_1\le m\le n_2$. However, the gain in computation time by a restriction to the EIBZ($\mathbf{q}$) usually outweighs the overhead from the summation over the degenerate states by far. For symmetry groups with time-reversal symmetries, the derivation can be done analogously with a more general great orthogonality theorem.[36] The final result is identical to Eq. (54).

IV. TEST CALCULATIONS

We have implemented above algorithm in the computer program SPEX. In the following, we first show detailed convergence tests for Si and SrTiO₃. Silicon is a prototype semiconductor, for which many *GW* calculations already exist and which is therefore used as a benchmark material. Strontium titanate is a prototype transition-metal oxide, which crystallizes in the frequently occurring perovskite structure. It is currently explored as a high-κ dielectric and a promising barrier material in spintronics and nanoelectronics. The valence and the lowest conduction bands are formed by O $2p$ and Ti $3d$ states, respectively. We explicitly include the semicore $3s$ and $3p$ states of Ti as well as the $4s$ and $4p$ states of Sr with the help of local orbitals and take their contribution to the screening into account. All these states are accurately described by the FLAPW basis set. Additional local orbitals are used to improve the description of high-lying unoccupied states.[24] As reference, we also show an overview of *GW* results for a wide range of semiconductors including BaTiO₃ and compare them with experimental and theoretical values from the literature. Furthermore, the efficiency of our scheme is illustrated by calculations for diamond supercells containing 16 and 128 atoms.

The numerical procedure involves a number of convergence parameters, which determine the accuracy of convolutions in real space (MPB), reciprocal space ($\mathbf{k}$-point set), and the frequency domain. Since the latter two apply to essentially all electronic-structure methods, we concentrate mainly on the parameters for the MPB here. Specifically, we consider the cutoff parameters $L_{\max}$ for the angular momentum inside the MT spheres and $G'_{\max}$ for the IPWs as well as the threshold $v_{\min}$ for the optimization of the MPB according to Sec. III F. We also discuss the convergence with respect to the number of unoccupied states for the summations in Eqs. (22) and (26). All calculations are done with a $4\times4\times4$ $\mathbf{k}$-point set and the local-density approximation (LDA) (Ref. 37) for the exchange-correlation functional at the DFT level.

The MPB is designed as a basis for the products of the wave functions [Eq. (14)], for which MT functions with angular momenta as large as $l_{\max}=8$ or even larger are typically taken into account. As a consequence, an exact representation of the products inside the spheres requires spherical harmonics at least up to $2l_{\max}$. However, the high angular momenta in the original FLAPW basis are mostly needed to ensure an accurate matching to the IPWs and contribute little to the actual wave functions. In fact, we find that the cutoff parameter $L_{\max}$ for the MPB can be chosen much smaller than $2l_{\max}$ and, indeed, even smaller than $l_{\max}$. Figure 1 shows the convergence of the quasiparticle transitions $\Gamma_{25'\mathrm{v}}\rightarrow\Gamma_{15\mathrm{c}}$ and $\Gamma_{25'\mathrm{v}}\rightarrow X_{1\mathrm{c}}$ in (a) Si as well as
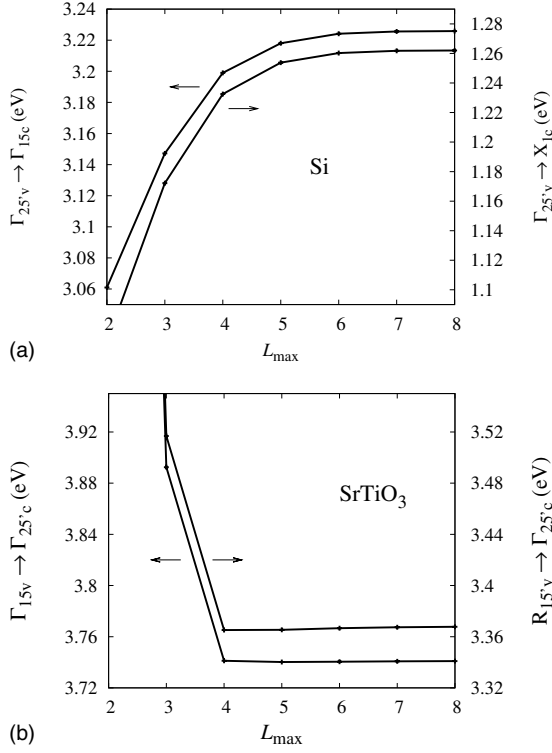
FIG. 1. Convergence of (a) the $\Gamma_{25'v} \rightarrow \Gamma_{15c}$ and $\Gamma_{25'v} \rightarrow X_{1c}$ gaps of Si and (b) the $\Gamma_{15v} \rightarrow \Gamma_{25'c}$ and $R_{15'v} \rightarrow \Gamma_{25'c}$ gaps of SrTiO$_3$ as a function of the MPB cutoff parameter L_{max} for the angular quantum number.
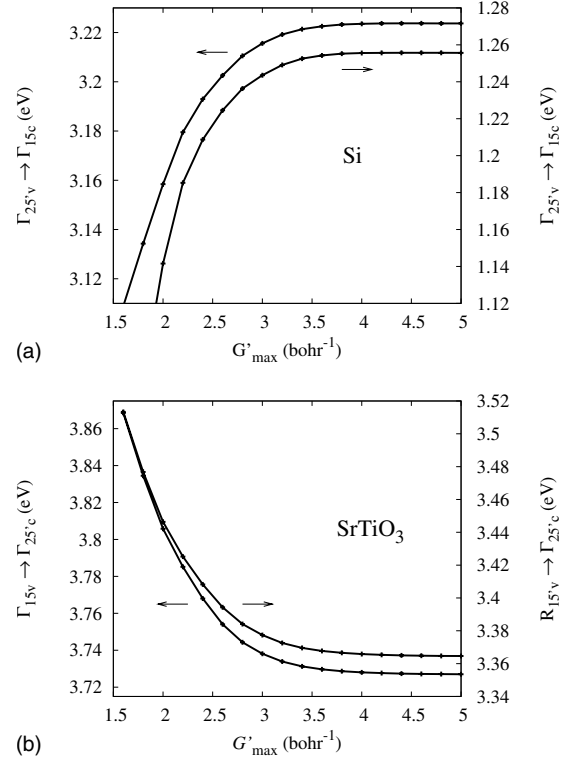

FIG. 2. Convergence of (a) the $\Gamma_{25'v} \rightarrow \Gamma_{15c}$ and $\Gamma_{25'v} \rightarrow X_{1c}$ gaps of Si and (b) the $\Gamma_{15v} \rightarrow \Gamma_{25'c}$ and $R_{15'v} \rightarrow \Gamma_{25'c}$ gaps of SrTiO$_3$ as a function of the MPB cutoff parameter G'_{max} for the IPWs.

$\Gamma_{15v} \rightarrow \Gamma_{25'c}$ and $R_{15'v} \rightarrow \Gamma_{25'c}$ in (b) SrTiO$_3$ with respect to L_{max}. Convergence to within 0.01 eV is already attained with $L_{max} = 5$ for Si and $L_{max} = 4$ for SrTiO$_3$. With these cutoff values, the MPB contains 292 and 853 MT functions, respectively.

A similar statement can be made about the convergence parameter G'_{max} for the IPWs. Although an exact representation requires twice the wave-function cutoff G_{max}, which we choose as 3.6 bohr^{-1} for Si and 4.3 bohr^{-1} for SrTiO$_3$ (giving rise to around 200 and 550 augmented plane waves, respectively), again a much smaller cutoff parameter is sufficient for the products. Figure 2 confirms that convergence to within 0.01 eV is achieved with $G'_{max} = 2.7$ bohr^{-1} and $G'_{max} = 3.2$ bohr^{-1} for Si and SrTiO$_3$, respectively, which yield around 100 and 250 IPWs in the MPB. In general, we find that the ratio $G'_{max}/G_{max} \approx 0.75$ can be used as a rule of thumb and works well for all materials considered here.

In Fig. 3, we show the convergence of the gap energies of Si and SrTiO$_3$ with respect to the threshold value v_{min} defined in Sec. III F. If the MPB was complete, the eigenvalues of the Coulomb matrix would be given by the Fourier transform $v_G(\mathbf{k}) = 4\pi / |\mathbf{k} + \mathbf{G}|^2$. With this in mind, the threshold value can be reformulated in terms of a cutoff in reciprocal space $|\mathbf{k} + \mathbf{G}| \leq \sqrt{4\pi/v_{min}}$, very similar to that for the IPWs discussed above. Therefore, it is reasonable to show the convergence in terms of this cutoff value, even though the MPB is only complete in the subspace spanned by the wave-function products, of course, and the Fourier transform $v_G(\mathbf{k})$ is hence only an estimate for the eigenvalues.

Figure 3(a) shows the convergence of the quasiparticle transitions for Si with respect to $\sqrt{4\pi/v_{min}}$. We observe that the values are converged to within 0.01 eV around 3.5 bohr^{-1}, which corresponds to $v_{min} = 1.9$ ha. With these values the rank of the matrix W (see Fig. 4) is reduced from 392 (the full MPB) to around 75 and the computation time from 140 to 42 s on an Intel Xeon (2.66 GHz, 4 MB cache) work station. Interestingly, the curve of the indirect transition in Fig. 3(a) exhibits a sudden step between 5.25 and 5.5 bohr^{-1}, where the gap energy changes by 4 meV. A similar but much smaller step of 0.7 meV can also be observed in the direct transition. Noting the simplified estimates $v_G(\mathbf{k})$ for the eigenvalues, this can be attributed to a shell of reciprocal vectors with length $|\mathbf{k} + \mathbf{G}|$ that enter between the radii 5.25 and 5.5 bohr^{-1} and give a sizable contribution. Although simplified, this is the correct picture because the true set of eigenvalues $v_\mu(\mathbf{k})$ usually contains many groups of degenerate eigenvalues, especially at high-symmetry points $\mathbf{k}$ in the BZ. By analogy, these groups can be viewed as shells of $\mathbf{k} + \mathbf{G}$ vectors in reciprocal space.

In SrTiO$_3$, the gap energies converge somewhat less smoothly but systematically. From Fig. 3(b), we see that after 5.3 bohr^{-1} the energies change by less than 0.01 eV. We note that the convergence criterion of 0.01 eV is quite ambitious for *GW* calculations. If we relax this criterion to, e.g., 0.05 eV, which should be sufficient for most studies, considerably smaller cutoffs suffice.

Equations (22) and (26) involve a summation over the unoccupied states $\varphi_{n'\mathbf{q}+\mathbf{k}}^\sigma(\mathbf{r})$. In practice, we must truncate
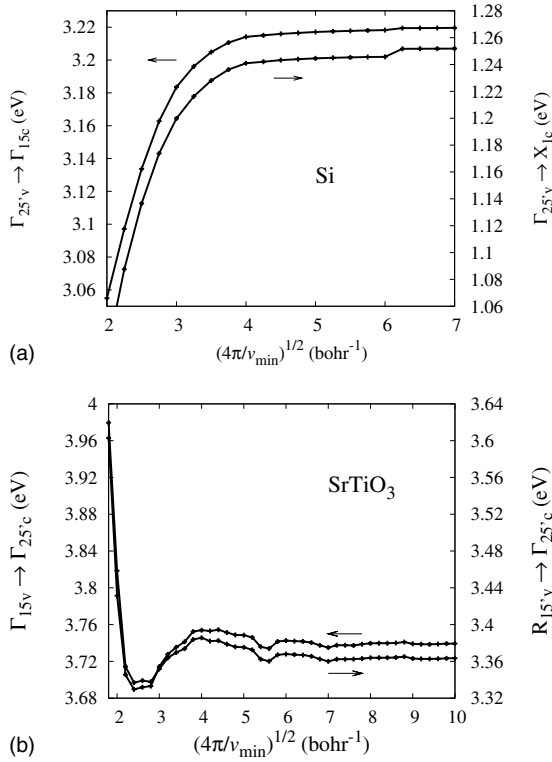
(a)

(b)

FIG. 3. Convergence of (a) the $\Gamma_{25'v} \rightarrow \Gamma_{15c}$ and $\Gamma_{25'v} \rightarrow X_{1c}$ gaps of Si and (b) the $\Gamma_{15v} \rightarrow \Gamma_{25'c}$ and $R_v \rightarrow \Gamma_{25'c}$ gaps of SrTiO$_3$ as a function of $\sqrt{4\pi/v_{min}}$.

this sum at some maximal band index N'. It is well known that a proper convergence of the *GW* quasiparticle energies requires very many unoccupied states.[24,38] While for SrTiO$_3$, a relatively modest number of 200 states is sufficient, the band gaps of Si, in particular, the indirect one, are more difficult to converge. Recently, Bruneval and Gonze[39] proposed an approximate scheme that corrects for the neglect of the states with indices $n' > N'$ and only involves the states with $n' \leq N'$. They showed that this *extrapolar* correction reduces the number of states needed for convergence considerably with only a small computational overhead. In short, all states $n' > N'$ are placed on a fixed energy above all others, which allows to take the energy denominator of Eqs.
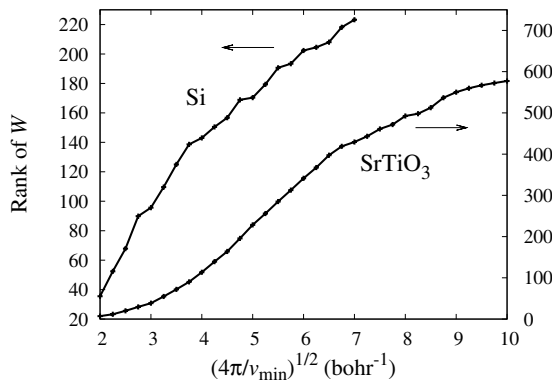

FIG. 4. Rank of the matrix W for the screened interaction, which equals the number of basis functions after the optimization, for Si and SrTiO$_3$ as a function of $\sqrt{4\pi/v_{min}}$.
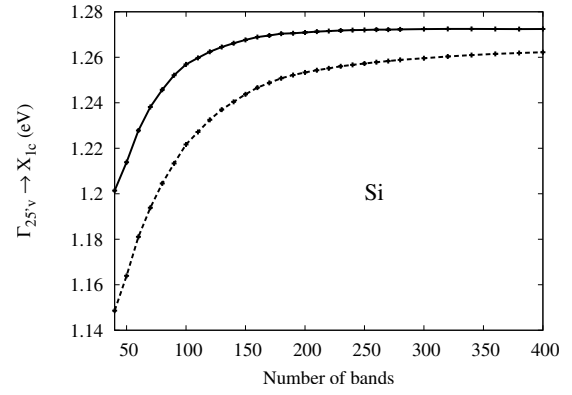

FIG. 5. Convergence of the $\Gamma_{25'v} \rightarrow X_{1c}$ gap of Si with respect to the number of bands used in the construction of the polarization function as well as the self-energy with (solid line) and without the extrapolar correction (dashed line).

(22) and (26) out of the sum over n' and to use the completeness relation for the one-particle states $\varphi_{n'q+k}^{\sigma}(\mathbf{r})$. The final expression can then be evaluated only with the states $n' \leq N'$. We have implemented this scheme in an all-electron code. Contrary to Ref. 39, we do not employ a plasmon-pole model, though, but use the full matrix of the screened interaction in the correction. As shown in Fig. 5, we find a considerably improved convergence with respect to the number of bands, too. The fixed energy for the bands $n' > N'$ is placed 16 Ry (217.7 eV) above the maximal energy of the bands $n' \leq N'$. However, all other results in this paper were obtained with the conventional summation. We note that the LAPW basis is a relatively small and accurate basis for the occupied states. In order to get enough unoccupied states for *GW* calculations, it is therefore often necessary to extend the LAPW basis by increasing the reciprocal cutoff radius G_{max} and introducing additional local orbitals.

For reference, we list the fundamental LDA and *GW* band gaps for a variety of semiconductors and insulators in Table I, together with experimental and other theoretical values for comparison. The latter are calculated with the LMTO (Ref. 12) and the PAW method (Ref. 40). Our own results for the fundamental band gaps are converged to within 0.01 eV with respect to the numerical parameters, including the BZ sampling. We find that an accurate description of high-lying unoccupied states with additional local orbitals is crucial for properly converged *GW* results. The core states can also have a sizable effect on electron correlation and the resulting band gaps. For example, inclusion of the cation 2s and 2p states of MgO and NaCl changes their band gaps by as much as 0.2 eV. Semicore states (e.g., Mg 2p) are described with local orbitals while deeper core states (e.g., Mg 2s) are treated as dispersionless bands, whose wave functions are confined to the MT spheres. Overall our LDA and *GW* values agree very well with those of Ref. 40 but somewhat less so with the older Ref. 12. As expected, the LDA considerably underestimates the band gaps. The *GW* self-energy corrects this underestimation in such a way that the results come very close to the measured values. However, there is still a slight underestimation in most cases. It has been suggested that a self-consistent scheme could improve the *GW* values

TABLE I. Fundamental *GW* band gaps for a variety of semiconductors and insulators compared with experimental and theoretical values from the literature. We also indicate the LDA eigenvalue gaps. All values are in electron volts.

	LDA	*GW*	LDA[a]	*GW*[a]	LDA[b]	*GW*[b]	Expt.
Ge	0.02	0.75	−0.08	0.57			0.74[c]
Si	0.62	1.11	0.46	0.90	0.62	1.12	1.17[d]
GaAs	0.29	1.31	0.33	1.31	0.49	1.30	1.63[d]
CdS	1.17	2.18			1.14	2.06	2.58[e]
GaN	1.67	2.83	1.81	3.03	1.62	2.80	3.27[f]
SrTiO$_3$	1.80	3.36					3.25[g]
BaTiO$_3$	2.18	3.18					3.3[h]
CaSe	2.04	3.63					3.85[i]
C	4.15	5.62	4.11	5.49	4.12	5.50	5.48[d]
BN	4.35	6.20			4.45	6.10	5.97[j]
MgO	4.64	7.17	4.85	6.77	4.76	7.25	7.83[k]
NaCl	4.90	7.53					8.5[l]

[a]Reference 12.
[b]Reference 40.
[c]Reference 41.
[d]Reference 42.
[e]Reference 43.
[f]Reference 44.
[g]Reference 45.
[h]Reference 46.
[i]Reference 47.
[j]Reference 48.
[k]Reference 49.
[l]Reference 50.

further.[40,51] The starting point is then optimized in such a way that the resulting one-particle orbitals are as close as possible to the quasiparticle wave functions; in particular, closer than those from standard local or semilocal functionals. In this way, the first-order perturbative correction [Eq. (4)], where the quasiparticle wave functions are approximated by the one-particle orbitals, is better justified. However, self-consistent *GW* calculations are computationally very expensive. When compared with the electronic self-energy, the most obvious source of errors in the local and semilocal DFT functionals is the missing self-interaction correction, which influences the shape of the KS wave functions. Therefore, better results might alternatively be obtained if one uses a functional that treats electronic exchange more accurately, e.g., the exact exchange functional within the optimized-effective-potential method or hybrid functionals.[52,53] These approaches go beyond the scope of the present paper. Nevertheless, we note that the numerical procedure for the *GW* approximation presented here is independent of the starting point and could also be applied within a self-consistent scheme or to functionals containing an exact exchange term.

As the *GW* approximation contains the exact exchange self-energy, it does not suffer from the unphysical self-interaction error present in local-density functionals such as the LDA. Localized states are most strongly affected by this error and appear too high in energy within the LDA. Thus,
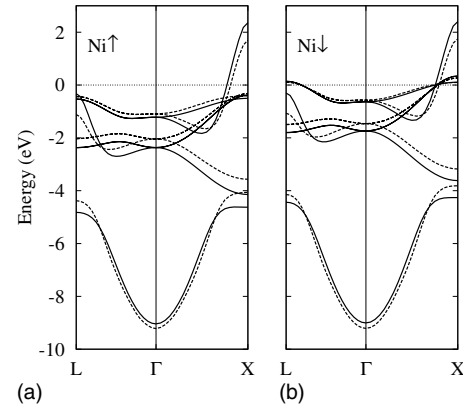

FIG. 6. Band structure of Ni calculated by the LSDA (dashed lines) and the *GW* approximation (solid lines) for majority (left panel) and minority spin (right panel). The Fermi energy is set to zero.

the absence of the self-interaction error in the *GW* approximation should lead to an improved description of these states. In fact, the quasiparticle levels of the localized Ga and As 3*d* semicore states in gallium arsenide lie 2.1 and 3.1 eV deeper than their LDA counterparts. Their theoretical binding energies are 16.9 and 38.4 eV, respectively, which still underestimates the experimental values of 18.82 and 40.76 eV from x-ray photoemission spectroscopy.[54] It has been shown that self-consistent calculations can further improve the *d*-band positions.[40,51]

In Fig. 6, we show the local-spin-density approximation (LSDA) (Ref. 37) and *GW* band structures for ferromagnetic Ni. The self-energy correction was calculated with a $8 \times 8 \times 8$ sampling of the BZ. Convergence was tested with a $10 \times 10 \times 10$ set. While for the semiconductors and insulators treated so far a model function [Eq. (27)] for the correlation self-energy with three poles, i.e., $N_p = 3$, was sufficient, we must use a five-pole function in the case of Ni to reproduce the values that we get from the reference contour-integration method. A comparison of the LSDA and *GW* band structures shows that the self-energy correction is strongly state and **k** dependent whereas in the case of materials with a band gap, the quasiparticle shifts are more or less uniform over the BZ but different for occupied and unoccupied states. The *GW* quasiparticle correction reduces the occupied *d*-band width from about 4.0 eV in the LSDA to 3.2 eV, which is in accordance with x-ray photoemission experiments.[55] On the other hand, the exchange splitting is hardly improved. There is only a slight reduction, which cannot account for the large overestimation within LSDA. The reason for this shortcoming is that the *GW* self-energy lacks two-particle vertex corrections, which give rise to spin-dependent screening and thus to a different correction for spin-up and spin-down states. Furthermore, the 6 eV satellite, which originates from a virtual bound two-hole excitation, cannot be described within the *GW* approximation for the same reason. Our *GW* band structure compares very well with an early work within the LAPW method[9] but less well with a more recent LMTO calculation.[56] About this discrepancy we can only speculate. It might be attributed to a less accurate description of unoccupied states within the LMTO basis or to the usage of the

TABLE II. Computational time for the calculation of quasiparticle shifts of diamond in the conventional ($1 \times 1 \times 1$) and supercell ($2 \times 2 \times 2$ and $4 \times 4 \times 4$) geometries. For the former we also show corresponding timings without use of symmetry ("No") and with restricted use ("Only IS" and "Only IBZ") as well as the effect of the MPB optimization with a threshold value v_{min}.

Geometry	Atoms	k mesh	Symmetry	v_{min}	CPU	Time
$1 \times 1 \times 1$	2	$4 \times 4 \times 4$	No		5 min	52 s
			Only IS		3 min	34 s
			Only IBZ			30 s
			Yes			11 s
			Yes	0.65		5 s
$2 \times 2 \times 2$	16	$2 \times 2 \times 2$	Yes	0.65	14 min	15 s
$4 \times 4 \times 4$	128	$1 \times 1 \times 1$	Yes	0.65	34 h	11 min

offset-Γ method in Ref. 56, in which the numerically important region around the center of the BZ is treated only approximately.

In order to demonstrate the efficiency of the code, we show the computational time for calculating quasiparticle shifts for diamond in the conventional unit cell ($1 \times 1 \times 1$) containing two atoms as well as in $2 \times 2 \times 2$ and $4 \times 4 \times 4$ supercell geometries containing 16 and 128 atoms, respectively. We choose the parameters so that all three calculations yield identical results. For example, the **k** mesh contains $4 \times 4 \times 4$, $2 \times 2 \times 2$, and $1 \times 1 \times 1$ points, respectively. The other parameters are determined to ensure convergence to within 0.01 eV. The computation times on a single CPU are given in Table II. While the calculation of the quasiparticle shifts takes only 5 s for the conventional unit cell, even the treatment of supercells containing 16 and 128 atoms only consumes affordable 0.24 and 34.2 h of computation time, respectively.

In the case of the conventional unit cell ($1 \times 1 \times 1$), we also demonstrate the efficiency gain achieved by exploiting the symmetry according to Sec. III G and by using a threshold parameter v_{min} as in Sec. III F. If symmetry is not used at all, then the computation of the quasiparticle shifts takes nearly 6 min. The diamond structure exhibits inversion symmetry (IS), which allows to define the bare and screened Coulomb matrices as real symmetric instead of complex Hermitian quantities after a symmetrization of the MT functions as briefly described in Sec. III B (for more details, see Ref. 27). This reduces the computation time roughly by a factor of 2 ("Only IS"). If we next calculate the screened interaction only in the irreducible wedge of the BZ, i.e., at eight **k** points instead of 64, the computation time goes down further to 30 s ("Only IBZ"). The gain is slightly less than a factor of 8 because the BZ summation in Eq. (25) must still be performed with all 64 **k** points. We can only restrict this summation and the sum over **q** in Eq. (22) if we use the extended IBZ (EIBZ) as explained in Sec. III G, which leads to further time savings of a factor of 3. Compared to the first calculation, the usage of symmetry thus leads to a 32 times faster execution without loss of accuracy. By introducing a threshold parameter $v_{min}=0.65$ for the optimization of the MPB, we can even reduce the computation time further to only 5 s, gaining an overall factor of 70.

V. CONCLUSIONS

In this paper, we described an implementation of the *GW* approximation for the electronic self-energy within the all-electron full-potential linearized augmented-plane-wave method.[25] We employ a mixed product basis, which is specifically designed for the representation of wave-function products and retains the full accuracy of the all-electron framework. As all-electron *GW* calculations have so far been prohibitive for large systems due to the computational cost, we presented ways to speed up the calculations considerably so that supercell calculations for defect systems, nanowires, interface, or surface structures become feasible. As a demonstration, we showed that our computer code can treat 128 carbon atoms in a diamond supercell. This was achieved by exploiting spatial and time-reversal symmetries in the evaluation of the polarization function and the self-energy. Both quantities exhibit a **k** dependence and also involve a BZ summation. While we only need to consider **k** points in the IBZ for the former, the latter can be restricted to an EIBZ, which accelerates the code considerably. If the system exhibits inversion symmetry, a symmetrization of the MT part of the mixed product basis leads to real symmetric instead of complex Hermitian response matrices, which reduces the CPU time and memory demand. Furthermore, for the correlation part of the self-energy, we can apply an optimization of the mixed product basis that involves a basis transformation to the eigenvectors of the Coulomb matrix. By neglecting eigenvectors with eigenvalues below a certain threshold value, we only retain the dominant part of the bare electron-electron interaction. The threshold value then becomes a convergence parameter. This optimization reduces the matrix sizes of response quantities such as the screened interaction, again giving rise to a speed up of the calculation. We note that no further approximations such as plasmon-pole models or a range separation of the interaction potential are introduced, and the anisotropy of the screening at **k**=0 is fully taken into account. The divergence of the bare and the screened interaction potential in the limit **k**→0 is treated analytically while zeroth-order correction terms are derived with the help of **k**·**p** perturbation theory. This procedure gives rise to a fast **k**-point convergence, which is particularly important for *GW* calculations.

We showed convergence tests for silicon and strontium titanate as a prototype semiconductor and transition-metal oxide, respectively, to illustrate the accuracy of the mixed product basis and its optimization with a threshold value for the Coulomb eigenvalues. The results already converge with relatively modest parameters. For example, for the angular momenta inside the MT spheres and the plane-wave representation in the IR, cutoff values well below the exact limit (i.e., twice the corresponding FLAPW cutoffs) are sufficient for convergence of the gap energies to within 0.01 eV. In fact, the cutoff values can even be chosen smaller than the FLAPW cutoffs. For reference, we reported the fundamental *GW* band gaps for a variety of semiconductors and insulators. Our results are in good agreement with recent *GW* calculations based on the PAW method and with experiments, although there is a somewhat larger discrepancy with older *GW* results obtained within the LMTO method. For ferro-

magnetic Ni, we find that the *GW* self-energy reduces the *d*-band width from 4.0 to 3.2 eV in very good agreement with experiment but hardly improves the overestimation of the exchange splitting within LSDA. These results are in accordance with previous calculations.

For simplicity, we have restricted ourselves to the non-self-consistent approach. However, with the numerical procedure presented here we are prepared to follow Ref. 51 and extend the method to the quasiparticle self-consistent scheme. Within this approach, the full self-energy matrix including off-diagonal elements is needed. The extension of

the numerical procedure developed in the present paper to these elements is straightforward.

*c.friedrich@fz-juelich.de

[1] W. G. Aulbur, L. Jönsson, and J. W. Wilkins, Solid State Phys. **54**, 1 (1999).

[2] S. L. Adler, Phys. Rev. **126**, 413 (1962); N. Wiser, *ibid.* **129**, 62 (1963).

[3] L. Hedin, Phys. Rev. **139**, A796 (1965).

[4] M. S. Hybertsen and S. G. Louie, Phys. Rev. Lett. **55**, 1418 (1985).

[5] R. W. Godby, M. Schlüter, and L. J. Sham, Phys. Rev. Lett. **56**, 2415 (1986).

[6] M. S. Hybertsen and S. G. Louie, Phys. Rev. B **34**, 5390 (1986).

[7] R. W. Godby, M. Schlüter, and L. J. Sham, Phys. Rev. B **35**, 4170 (1987).

[8] N. Hamada, M. Hwang, and A. J. Freeman, Phys. Rev. B **41**, 3620 (1990).

[9] F. Aryasetiawan, Phys. Rev. B **46**, 13051 (1992).

[10] W. Ku and A. G. Eguiluz, Phys. Rev. Lett. **89**, 126401 (2002).

[11] M. Usuda, N. Hamada, T. Kotani, and M. van Schilfgaarde, Phys. Rev. B **66**, 125101 (2002).

[12] T. Kotani and M. van Schilfgaarde, Solid State Commun. **121**, 461 (2002).

[13] A. Yamasaki and T. Fujiwara, Phys. Rev. B **66**, 245108 (2002).

[14] S. V. Faleev, M. van Schilfgaarde, and T. Kotani, Phys. Rev. Lett. **93**, 126406 (2004).

[15] B. Arnaud and M. Alouani, Phys. Rev. B **62**, 4464 (2000).

[16] S. Lebègue, B. Arnaud, M. Alouani, and P. E. Bloechl, Phys. Rev. B **67**, 155208 (2003).

[17] M. Shishkin and G. Kresse, Phys. Rev. B **74**, 035101 (2006).

[18] A. Ernst, M. Lüders, P. Bruno, W. M. Temmerman, and Z. Szotek (unpublished).

[19] P. Puschnig and C. Ambrosch-Draxl, Phys. Rev. B **66**, 165105 (2002).

[20] C. Friedrich, A. Schindlmayr, and S. Blügel, Comput. Phys. Commun. **180**, 347 (2009).

[21] W. Kohn and L. J. Sham, Phys. Rev. **140**, A1133 (1965).

[22] O. K. Andersen, Phys. Rev. B **12**, 3060 (1975).

[23] D. Singh, Phys. Rev. B **43**, 6388 (1991).

[24] C. Friedrich, A. Schindlmayr, S. Blügel, and T. Kotani, Phys. Rev. B **74**, 045104 (2006).

[25] Further details available from http://www.flapw.de

[26] F. Aryasetiawan and O. Gunnarsson, Phys. Rev. B **49**, 16214 (1994).

[27] M. Betzinger, C. Friedrich, and S. Blügel (unpublished).

[28] L. Dagens and F. Perrot, Phys. Rev. B **5**, 641 (1972).

[29] H. N. Rojas, R. W. Godby, and R. J. Needs, Phys. Rev. Lett. **74**, 1827 (1995); M. M. Rieger, L. Steinbeck, I. D. White, H. N. Rojas, and R. W. Godby, Comput. Phys. Commun. **117**, 211 (1999).

[30] R. W. Godby, M. Schlüter, and L. J. Sham, Phys. Rev. B **37**, 10159 (1988); F. Aryasetiawan, in *Advances in Condensed Matter Science*, edited by V. I. Anisimov (Gordon and Breach, New York, 2000).

[31] J. Rath and A. J. Freeman, Phys. Rev. B **11**, 2109 (1975).

[32] S. Baroni and R. Resta, Phys. Rev. B **33**, 7017 (1986).

[33] S. Massidda, M. Posternak, and A. Baldereschi, Phys. Rev. B **48**, 5058 (1993).

[34] C. Freysoldt, P. Eggert, P. Rinke, A. Schindlmayr, R. W. Godby, and M. Scheffler, Comput. Phys. Commun. **176**, 1 (2007).

[35] *Ergebnisse in der Elektronentheorie der Metalle*, edited by P. Ziesche and G. Lehmann (Akademie/Springer, Berlin, 1983).

[36] S. K. Kim, *Group Theoretical Methods and Applications to Molecules and Crystals* (Cambridge University Press, Cambridge, 1999).

[37] J. P. Perdew and A. Zunger, Phys. Rev. B **23**, 5048 (1981).

[38] M. L. Tiago, S. Ismail-Beigi, and S. G. Louie, Phys. Rev. B **69**, 125212 (2004).

[39] F. Bruneval and X. Gonze, Phys. Rev. B **78**, 085125 (2008).

[40] M. Shishkin and G. Kresse, Phys. Rev. B **75**, 235102 (2007).

[41] G. G. Macfarlane, T. P. McLean, J. E. Quarrington, and V. Roberts, Phys. Rev. **108**, 1377 (1957).

[42] T. C. Chiang and F. J. Himpsel, in *Electronic Structure of Solids: Photoemission Spectra and Related Data*, Landolt-Börnstein New Series, Group III Vol. 23A, edited by A. Goldmann and E.-E. Koch (Springer, Berlin, 1989).

[43] K. O. Magnusson, U. O. Karlsson, D. Straub, S. A. Flodström, and F. J. Himpsel, Phys. Rev. B **36**, 6566 (1987).

[44] H. Okumura, S. Yoshida, and T. Okahisa, Appl. Phys. Lett. **64**, 2997 (1994).

[45] K. van Benthem, C. Elsässer, and R. H. French, J. Appl. Phys. **90**, 6156 (2001).

[46] L. T. Hudson, R. L. Kurtz, S. W. Robey, D. Temple, and R. L. Stockbauer, Phys. Rev. B **47**, 1174 (1993).

[47] Y. Kaneko and T. Koda, J. Cryst. Growth **86**, 72 (1990).

[48] K. Watanabe, T. Taniguchi, and H. Kanda, Nature Mater. **3**, 404 (2004).

[49] R. C. Whited, C. J. Flaten, and W. C. Walker, Solid State Commun. **13**, 1903 (1973).

[50] R. T. Poole, J. G. Jenkin, J. Liesegang, and R. C. G. Leckey,

Phys. Rev. B **11**, 5179 (1975).

[51] T. Kotani, M. van Schilfgaarde, and S. V. Faleev, Phys. Rev. B **76**, 165106 (2007).

[52] P. Rinke, A. Qteish, J. Neugebauer, C. Freysoldt, and M. Scheffler, New J. Phys. **7**, 126 (2005).

[53] F. Bechstedt, F. Fuchs, and G. Kresse, Phys. Status Solidi B **246**, 1877 (2009).

[54] L. Ley, R. A. Pollak, F. R. McFeely, S. P. Kowalczyk, and D. A. Shirley, Phys. Rev. B **9**, 600 (1974).

[55] H. Höchst, S. Hüfner, and A. Goldmann, Z. Phys. B **26**, 133 (1977).

[56] A. Yamasaki and T. Fujiwara, J. Phys. Soc. Jpn. **72**, 607 (2003).